A Multibasin Residual-Mean Model for the Global Overturning Circulation

ANDREW F. THOMPSON

Environmental Science and Engineering, California Institute of Technology, Pasadena, California

ANDREW L. STEWART

Department of Atmospheric and Oceanic Sciences, University of California, Los Angeles, Los Angeles, California

TOBIAS BISCHOFF

Environmental Science and Engineering, California Institute of Technology, Pasadena, California

(Manuscript received 23 October 2015, in final form 27 May 2016)

ABSTRACT

The ocean's overturning circulation is inherently three-dimensional, yet modern quantitative estimates of the overturning typically represent the subsurface circulation as a two-dimensional, two-cell streamfunction that varies with latitude and depth only. This approach suppresses information about zonal mass and tracer transport. In this article, the authors extend earlier, zonally averaged overturning theory to explore the dynamics of a ''figure-eight'' circulation that cycles through multiple basins. A three-dimensional residual-mean model of the overturning circulation is derived and then simplified to a multibasin isopycnal box model to explore how stratification and diabatic water mass transformations in each basin depend on the basin widths and on deep and bottom-water formation in both hemispheres. The idealization to multiple, two-dimensional basins permits zonal mass transport along isopycnals in a Southern Ocean–like channel, while retaining the dynamical framework of residual-mean theory. The model qualitatively reproduces the deeper isopycnal surfaces in the Pacific Basin relative to the Atlantic. This supports a transfer of Antarctic Bottom Water from the Atlantic sector to the Pacific sector via the Southern Ocean, which subsequently upwells in the northern Pacific Basin. A solution for the full isopycnal structure in the Southern Ocean reproduces observed stratification differences between Atlantic and Pacific Basins and provides a scaling for the diffusive boundary layer in which the zonal mass transport occurs. These results are consistent with observational indications that North Atlantic Deep Water is preferentially transformed into Antarctic Bottom Water, which undermines the importance of an adiabatic, upper overturning cell in the modern ocean.

1. Introduction

The earliest schematics of the global ocean circulation (e.g., Broecker 1991) emphasized the three-dimensional nature of the overturning's closure with sinking in the North Atlantic and upwelling in the Pacific. This picture hinges on the zonally unbounded regions of the Southern Ocean, enabling exchange between the ocean basins via the Antarctic Circumpolar Current (ACC). The formation of Antarctic Bottom Water (AABW), and thus the potential for multiple overturning cells, was often excluded in these early schematics. More recent quantitative estimates of the overturning circulation (OC), from both observations and models, represent the OC as a streamfunction that varies with latitude and either depth or density (Speer et al. 2000; Lumpkin and Speer 2007). This depiction hides information about zonal components of ocean transport as well as zonal variations in stratification and meridional transport. These analyses typically present the ocean's overturning circulation as two closed cells: one associated with the formation of North Atlantic Deep Water (NADW) and the other with the formation of AABW.

Recently, Talley (2013) has argued, based on observed water mass distributions, that this two-cell structure is a consequence of collapsing the three-dimensional ocean circulation onto a two-dimensional streamfunction. To

Corresponding author address: Andrew F. Thompson, Environmental Science and Engineering, California Institute of Technology, 1200 E California Blvd., MC 131-24, Pasadena, CA 91125.
E-mail: andrewt@caltech.edu

DOI: 10.1175/JPO-D-15-0204.1

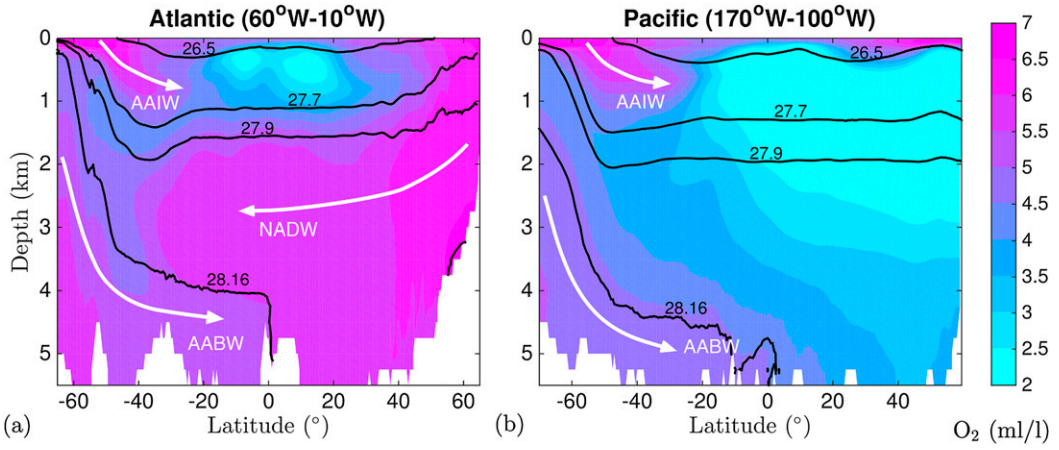

FIG. 1. Asymmetry in the zonal-mean stratification and major water mass export between (a) the Atlantic (60°–10°W) and (b) the Pacific (170°–100°W). Colors show dissolved oxygen (ml l^{-1}). Black contours show the neutral density surfaces γ^n = 26.5, 27.7, 27.9, and 28.16 kg m^{-3}, which approximately separate the major water masses. White arrows indicate the export of Antarctic Intermediate Water (AAIW), NADW, and AABW in each basin.

illustrate this point, in Fig. 1, we present the zonally averaged dissolved oxygen distribution and selected neutral density contours in the Atlantic and Pacific sectors. This highlights asymmetries between the major ocean basins, most notably the export of NADW from the North Atlantic and the deeper isopycnal surfaces in the Pacific sector. Ferrari et al. (2014) argue that in the present day, the ocean's overturning circulation is better described by a single continuous loop, as shown schematically in Fig. 2. A single overturning loop requires exchange between a diffusively dominated Pacific Basin and an Atlantic Basin that is hypothesized to have closed adiabatic circulation pathways when isopycnals outcrop in both hemispheres. The focus of this study is a dynamical assessment of constraints on basin-mean transport and stratification as well as the diabatic closure of a three-dimensional circulation.

The distinction between an adiabatic OC, in which significant water mass modification occurs only in the high-latitude surface ocean, and a diffusive OC, closed by interior diapycnal mixing, has been addressed by highlighting the unique properties of a periodic Southern Ocean (Marshall and Radko 2003). Southern Ocean wind forcing permits a mechanically controlled OC that is thermally indirect (Wolfe and Cessi 2010, 2014) when density surfaces outcrop in both Northern and Southern

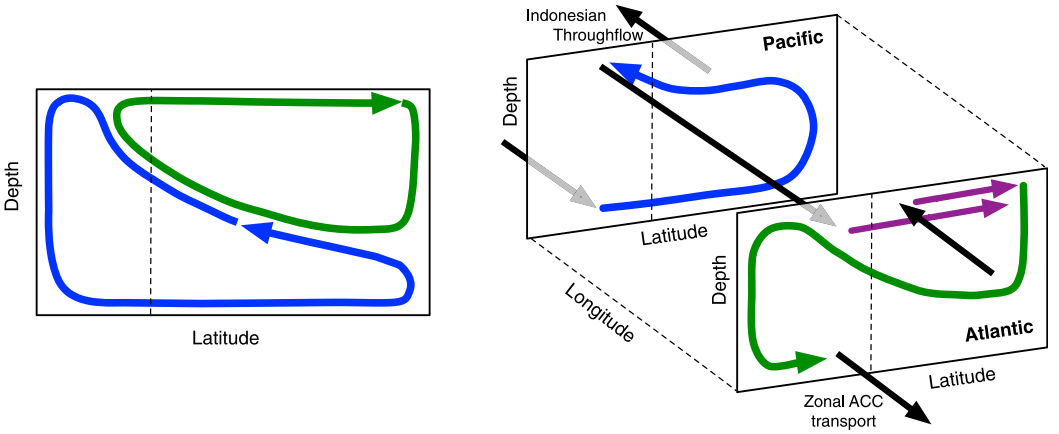

FIG. 2. (left) Schematic of the meridional overturning circulation in depth–latitude space. The green and blue curves are typically viewed as distinct overturning cells associated with North Atlantic Deep Water formation and Antarctic Bottom Water formation, respectively. (right) Idealized three-dimensional schematic of the overturning circulation following Talley (2013). Here, the overturning cycles through both the Atlantic and Pacific Basins, either through the Antarctic Circumpolar Current or the Indonesian Throughflow, before closing. Rather than two distinct cells, the overturning more closely approximates a single figure-eight loop.

Hemisphere high latitudes and interior diapycnal mixing is weak. In this regime, the strength of the OC is controlled by the magnitude of the wind stress over the ACC, the strength of eddy activity in the ACC region, and surface buoyancy forcing over the Southern Ocean. This has motivated a host of eddy-resolving ''sector'' models with a circumpolar channel appended to diffusive northern basins, intended to represent an upper cell of the OC (Wolfe and Cessi 2010; Morrison et al. 2011; Munday et al. 2013; Morrison and Hogg 2013).

In more idealized settings, Gnanadesikan (1999), Radko and Kamenkovich (2011), and Nikurashin and Vallis (2011, 2012) have sought to combine the classic abyssal recipes (Munk 1966) paradigm of the OC with adiabatic upwelling in the Southern Ocean by linking a periodic channel with a diffusively controlled northern basin. Eddy variability is included in such models through a residual-mean approach (Marshall and Radko 2003) that parameterizes eddy transport based on circumpolar-averaged properties of the ACC channel. However, the ACC supports dynamically significant zonal variations in meridional density structure (Naveira Garabato et al. 2014; Thompson and Garabato 2014), meridional transport (Naveira Garabato et al. 2011; Thompson and Sallée 2012; Dufour et al. 2015), and subduction from the mixed layer (Sallée et al. 2012). This zonal asymmetry is, in part, linked to the differing water mass distributions in the northern basins, for example, the presence of NADW in the Atlantic.

While residual-mean theory emphasizes the importance of interior eddy fluxes in the ACC, this interior circulation must also be consistent (in steady state) with surface water mass modification mediated by surface buoyancy forcing. Available air–sea buoyancy flux products (Large and Yeager 2009; Cerovečki et al. 2011) show large-scale, zonally asymmetric patterns with buoyancy gain in the Atlantic and Indian Oceans (outside of the Agulhas Retroflection) and weaker buoyancy fluxes (both positive and negative) in the Pacific. Tamsitt et al. (2016) have analyzed the surface heat budget in the Southern Ocean State Estimate (SOSE) model and showed that topographic steering and zonal asymmetry in air–sea exchange leads to even more dramatic zonal variability in the surface heat flux. In one of the only studies to address the dynamics of this zonal structure, Radko and Marshall (2006) introduced a perturbation with a mode-1 zonal wavenumber to the zonally averaged properties of the ACC. This resulted in an intensification of the overturning where the buoyancy gain is stronger. However, this model did not address the interaction between the Southern Ocean and northern basins. Recently, Jones and Cessi (2016) presented a two-layer, two-basin extension of Gnanadesikan (1999) that shows the three-dimensional circulation of an upper overturning cell. This model did not include AABW or explicitly discuss the closure of the overturning due to diabatic processes in the Southern Ocean.

This study seeks to bridge the gap between idealized, two-dimensional, residual-mean treatments of the OC and complex, fully three-dimensional models. To accomplish this we extend the two-dimensional, residual-mean model to three dimensions. We focus on a particular idealization of this model with two separate, two-dimensional basins that can exchange properties through the ACC or through the Indonesian Throughflow (ITF), as discussed in section 2 and appendix A. Even in two dimensions, analyzing and interpreting the three-dimensional OC is challenging, so we perform most of our analysis using an isopycnal ''box model'' simplification of the multibasin residual-mean equations derived in section 3. In section 4, we use this model to explore how interbasin differences in stratification and surface buoyancy forcing are connected via a ''figure-eight'' OC. In section 5, we show that a more thorough treatment of ACC isopycnals can more quantitatively explain the observed differences in stratification across the Atlantic and Pacific Basins. Discussion and conclusions are provided in sections 6 and 7.

2. Three-dimensional residual-mean model overview

This section provides a nontechnical introduction to and overview of the three-dimensional, residual-mean model. An essential feature of the three-dimensional overturning sketched in Fig. 2 is a connection between basins via the ACC. Zonal flow from one sector of the ACC to another can produce a convergence or a divergence of mass within each density class, which must be compensated by the meridional circulation in each sector. Zonal transport can also occur via a combination of the ITF and the Agulhas leakage, although this exchange is limited to near-surface density classes. Our objective is to derive a physically based conceptual model that can accommodate these features.

We adapt two-dimensional, residual-mean theory, which has been influential in documenting the importance of isopycnal upwelling in the Southern Ocean (Toggweiler and Samuels 1995; Marshall and Radko 2003; Marshall and Speer 2012), to multiple basins. In the absence of diabatic effects, buoyancy is materially conserved and thus the circulation is adiabatic. In developing a multibasin model of the overturning circulation, it is therefore most convenient to use isopycnal coordinates, which allow mass transferred from one basin to another to remain in the same density class. Below, we derive our multibasin, residual-mean model

by averaging along each sector of the ACC in isopycnal coordinates.[1]

Our starting point is the three-dimensional, residual-mean, buoyancy equation (Marshall and Radko 2006)

$$\frac{\partial \overline{b}}{\partial t} + J_x[\psi^{(x)}, \overline{b}] + J_y[\psi^{(y)}, \overline{b}] = \frac{\partial}{\partial z}\left(\kappa \frac{\partial \overline{b}}{\partial z}\right) + \frac{\partial \overline{B}}{\partial z}, \quad (1)$$

where bars indicate an average in time. Here, κ is a vertical diffusion coefficient that parameterizes diapycnal mixing due to internal wave breaking in the ocean interior. The Jacobians are defined as $J_x(p, q) \equiv p_x q_z - q_x p_z$ and $J_y(p, q) \equiv p_y q_z - q_y p_z$. Buoyancy forcing at the ocean surface is represented as a downward flux denoted as B. The mean buoyancy is advected by a vector residual streamfunction $\boldsymbol{\psi} = [\psi^{(x)}, \psi^{(y)}]$, from which the three-dimensional residual velocity $\mathbf{u}^\dagger$ can be reconstructed via

$$u^\dagger = -\frac{\partial \psi^{(x)}}{\partial z}, \quad v^\dagger = -\frac{\partial \psi^{(y)}}{\partial z}, \quad w^\dagger = \frac{\partial \psi^{(x)}}{\partial x} + \frac{\partial \psi^{(y)}}{\partial y}. \quad (2)$$

Appendix A provides a derivation of the transformation of (1) into isopycnal coordinates; (A6) is reproduced here:

$$\frac{\partial z}{\partial t} - \frac{\partial \psi^{(x)}}{\partial x}\bigg|_{\overline{b}} - \frac{\partial \psi^{(y)}}{\partial y}\bigg|_{\overline{b}} = -\frac{\partial}{\partial \overline{b}}\left[\kappa\left(\frac{\partial z}{\partial \overline{b}}\right)^{-1} + B\right]. \quad (3)$$

This equation describes the evolution of the depth z of a given mean density surface $\overline{b}$. The subscript $\overline{b}$ indicates that horizontal derivatives of the streamfunction should be taken at constant $\overline{b}$. Conceptually, this equation states that the rate of change of the mean isopycnal depth is equal to the component of the residual velocity normal to the mean isopycnal surface, unless diabatic effects (on the right-hand side) are present to permit a diapycnal residual flux. For an adiabatic interior and for steady state, (3) simplifies to

$$\frac{\partial \psi^{(x)}}{\partial x}\bigg|_{\overline{b}} + \frac{\partial \psi^{(y)}}{\partial y}\bigg|_{\overline{b}} = 0. \quad (4)$$

This states that in the steady adiabatic limit, the horizontal convergence of mass below a given isopycnal must vanish.

Even in isopycnal coordinates, (3) and (4) are difficult to solve in general because they are still fully three-dimensional equations. To simplify our analysis, we assume that within each sector of the ACC, the isopycnal depths are approximately uniform in the along-stream direction, with abrupt changes in the density structure in narrow zonal regions that separate different sectors of the ACC. Thompson and Garabato (2014) have argued that modifications to the density structure in the ACC occur rapidly across topographic features, where standing meanders generate strong mean flows and large eddy kinetic energy downstream. In Fig. 3, we show that the $\gamma = 27.9\,\mathrm{kg\,m^{-3}}$ neutral density surface, identified by Ferrari et al. (2014) as the isopycnal separating the "upper" and "lower" branches of the OC in the ACC, does indeed exhibit abrupt changes in depth across the ACC's major topographic features. The climatological isopycnal depth $z_{27.9}$, shown in Fig. 3a, was mapped to an along-stream coordinate system defined by the Subantarctic Front (SAF), Polar Front (PF), and Southern ACC Front (SACCF) from Orsi et al. (1995). At each longitude, we defined a modified latitudinal coordinate system centered on the PF, with latitudes to the north (south) of the PF rescaled by the half-width of the ACC, defined as the distance between the PF and the SAF (SACCF). Figure 3b was constructed by averaging $z_{27.9}$ latitudinally within three half-widths to the north and south of the PF at each longitude. Figure 3c was created by taking a streamwise average of several isopycnal depths in the Atlantic sector (red curve) and in the Indian, western Pacific, and eastern Pacific sectors (blue curve).

Motivated by the approximate along-stream invariance of the isopycnal depths away from major topographic features, in appendix A we show that averaging (3) along a zonal sector of the ACC leads to the following evolution equation for the sector-averaged isopycnal depth:

$$\frac{\partial z_i}{\partial t} - \frac{1}{L_i}(\Psi_i - \Psi_{i-1}) - \frac{\partial \psi_i}{\partial y} = -\frac{\partial}{\partial b}\left[\kappa_i\left(\frac{\partial z_i}{\partial b}\right)^{-1} + B_i\right]. \quad (5)$$

Here, different ACC sectors are distinguished by subscripts i with zonal extent L_i, for example $i = 1, \ldots, N$ for N ACC sectors, and $i - 1$ identifies the sector to the west of sector i. For a complete description of the notation, the reader is referred to appendix A. Equation (5) is similar to that derived by Su et al. (2014) to describe isopycnal height fluctuations in the Weddell Gyre. However, there is an additional contribution on the left-hand side because of the zonal flow into and out of the sector, quantified by the zonal transport streamfunction carrying flow out of the sector to the east Ψ_i and carrying flow in from the west Ψ_{i-1}. This allows

[1] Numerical discretizations of the residual-mean equations tend to be posed in z coordinates (e.g., Nikurashin and Vallis 2011, 2012; Stewart and Thompson 2013; Stewart et al. 2014). We choose isopycnal coordinates as the most natural framework, but similar equations may be derived using zonal averaging at fixed depth.

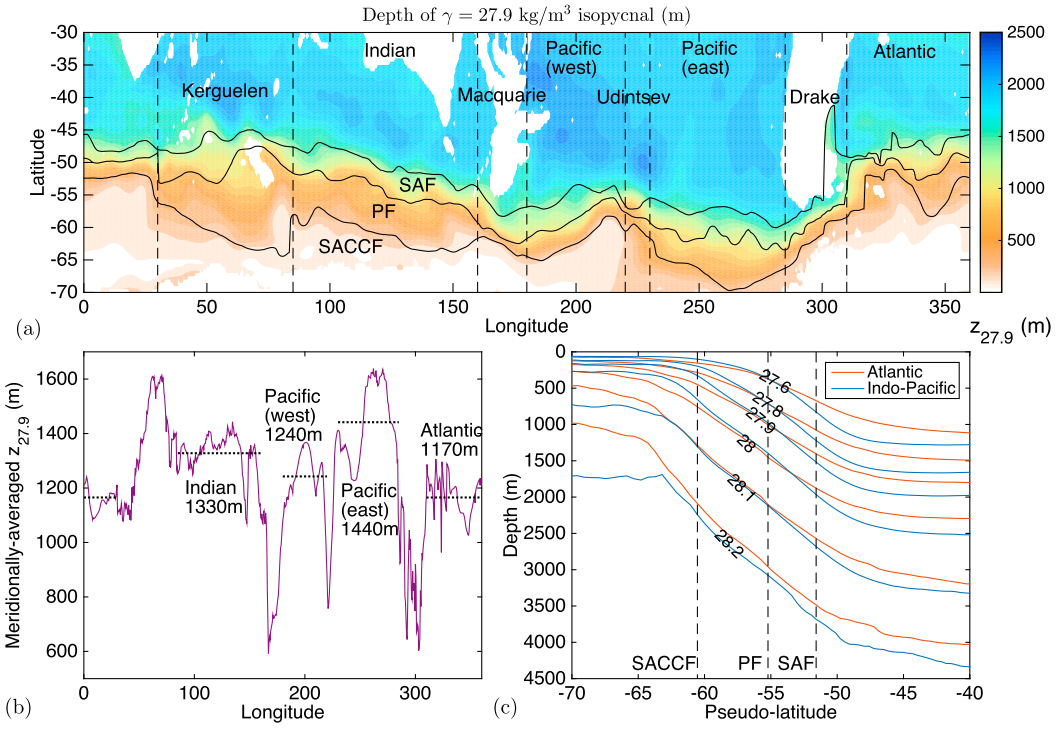

FIG. 3. (a) Climatological depth of the $\gamma = 27.9\,\mathrm{kg\,m^{-3}}$ isopycnal surface $z_{27.9}$ from Gouretski and Koltermann (2004). The solid black lines indicate the positions of the SAF, PF, and SACCF from Orsi et al. (1995), adjusted to be single-valued functions of longitude. The dashed lines highlight the separation of the Atlantic, Indian, and Pacific sectors of the ACC by topographic features. (b) Cross-stream-averaged depth of the same isopycnal surface as a function of longitude, with the cross- and along-stream-averaged depth in each basin indicated by dotted lines and text. (c) Along-stream-averaged depths of several neutral density surfaces in the Atlantic and Indo-Pacific sectors, presented as a function of a pseudolatitudinal coordinate constructed from the zonal-mean positions of the SAF, PF, and SACCF. Further details are provided in section 2.

zonal convergence/divergence of mass above and below the isopycnal to change the isopycnal depth.

In the following section, we build this representation of the overturning, constructed for the zonally periodic ACC, into a global, two-basin isopycnal box model with several density layers. This model employs a simplified treatment of the isopycnals in the ACC, approximating them as linear slopes. A more careful treatment of the isopycnal structure appears in section 5. The circulation and stratification in each basin are described by zonally averaged transports and buoyancy distributions. We use the box model to illustrate the figure-eight nature of the modern OC and its sensitivity to external parameters and forcing.

3. A residual-mean box model of the global overturning circulation

We begin our exploration of the three-dimensional, residual-mean model by applying a coarse discretization of (5) in the ACC and coupling it to diabatic processes that allow a full closure of the OC. The natural limit of this approach is an isopycnal box model. Diabatic processes include buoyancy forcing at the surface of the ACC and a diffusive upwelling in basins north of the ACC. High-latitude, deep- and bottom-water formation rates are prescribed for simplicity. We show that a consequence of the three-dimensional nature of the circulation is that the stratification differs between ocean basins.

The discussion is framed in terms of exchanges between Atlantic and Pacific Basins. However, references to the "Pacific" should be interpreted loosely as pertaining to the entire Indo-Pacific sector, as similar processes support the upwelling and southward return flow of AABW in the Indian and Pacific Basins (Talley 2013). The box model is also easily extended to include more than two basins.

This box model has commonalities with those derived by Gnanadesikan (1999), Shakespeare and Hogg (2012), Goodwin (2012), and Jones and Cessi (2016), which solve for the volume of different subsurface density

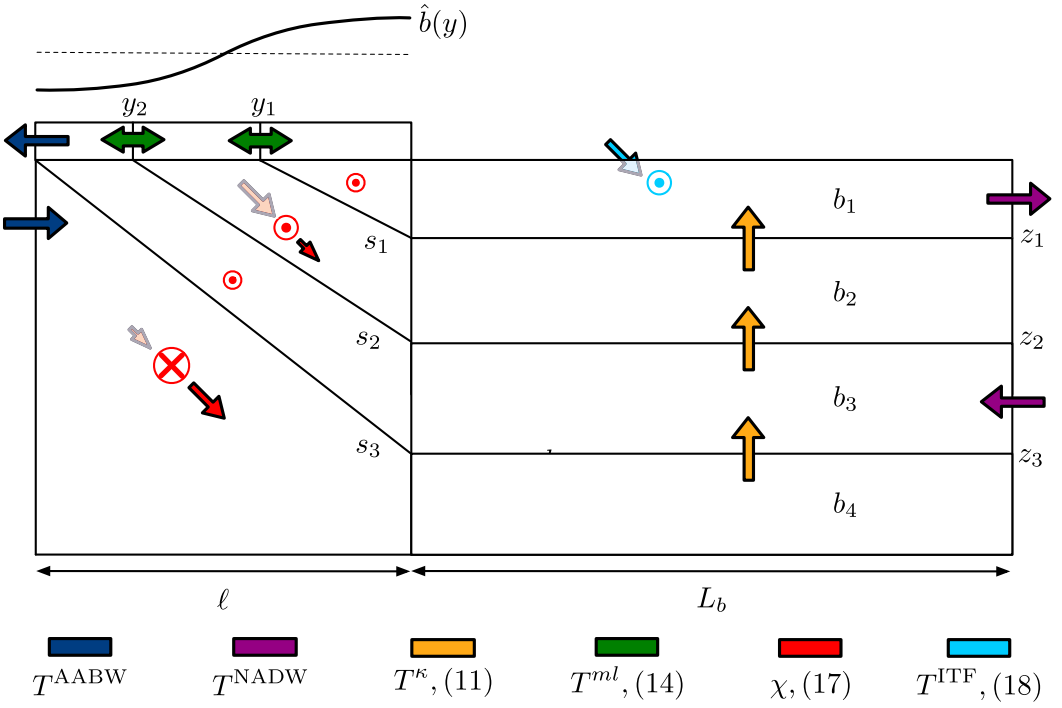

FIG. 4. Schematic of the Atlantic Basin for a multibasin, four-layer, isopycnal box model. The ACC sector spans $-\ell < y < 0$. Colored arrows indicate mass transports T described in the text; the legend below provides the equation number in the text that defines the transports in terms of model diagnostics. Bottom- and deep-water formation rates T^{AABW} and T^{NADW} are external parameters. Surface buoyancy forcing in the ACC arises from relaxation to a prescribed meridional buoyancy profile $\hat{b}(y)$ [(15)]. Zonal convergence of mass χ may occur in each layer of the ACC sector of the model; zonal transport via the Indonesian Throughflow T^{ITF} occurs in the uppermost layer.

classes that are dynamically linked to the circulation. In concept, the box model presented here is closest to Goodwin (2012), although it distinguishes between dynamics in the Pacific and Atlantic Basins and emphasizes the role of the ACC in allowing zonal convergence of mass in each sector. We first present the relationships that define the box model based on meridional, zonal, and diabatic transports. The definition of these transports in terms of the model diagnostics is largely based on parameterizations used in previous studies; the key addition is an expression for the zonal mass transport between the Atlantic and Pacific sectors.

Consider a model with two basins, $i = A, P$, and four density layers, $N = 4$ (see Fig. 4). A model with four layers can accommodate traditional lower and upper cells. Each layer interface is assigned an index $n = 0, 1, 2, \ldots, N$, where $n = 0$ and $n = N$ represent the surface and the flat ocean bottom, respectively. The nth density class is bounded by interfaces $n - 1$ and n. Each density layer is partitioned, meridionally, into a northern diffusive basin ($y > 0$) and a region spanning the ACC ($-\ell < y < 0$). The depth H of the ocean is fixed. The model solves for the depth of each layer interface in the basin region z_n, with $0 < z_n < -H$. The model also solves for the meridional position of the interface outcrop location in the ACC, y_n, with $-\ell < y_n < 0$. In this section, we consider a simplified system that captures the key aspects of a three-dimensional overturning. Thus, we impose uniform isopycnal slopes s in the ACC, which are determined from $s_n = z_n/y_n$; in section 5, we examine more realistic isopycnal distributions. For each interface, we impose the same slope in the Atlantic and Pacific Basins: $s_{A,n} = s_{P,n} = s_n$. For each layer, there are three unknowns: $z_{A,n}$, $y_{A,n}$ and $z_{P,n}$. Then, $y_{P,n}$ is determined from s_n.

In the following subsections, we make further approximations to the isopycnal residual-mean equation (5) to derive a box model representation of the OC. As a preface, we note that even in a box model formulation, representing the terms in (5) can be quite involved. The zonal streamfunction Ψ_i depends in general on the baroclinic structure of the ACC, which becomes more straightforward under our assumption of linear isopycnals. The meridional streamfunction ψ_i is in general decomposed into Ekman, eddy, and geostrophic components (see appendix A); in general the latter requires

that the model be able to represent the hydrostatic pressure. To avoid this level of complexity, we assume steady adiabatic flow in the ACC. Under this assumption, (5) may be integrated meridionally along any isopycnal to obtain

$$L_i[\psi]_{y_{i,n}}^{0} + \int_{y_{i,n}}^{0} \Psi_i \, dy - \int_{y_{(i-1),n}}^{0} \Psi_{i-1} \, dy = 0, \qquad (6)$$

for $i = A, P$. That is, the meridional overturning set by surface processes (at $y = y_{i,n}$) and in the northern basin (at $y = 0$) must match, unless there is a net zonal convergence/divergence above that isopycnal. As these terms can be determined from surface buoyancy forcing, diapycnal mixing, and the ACC stratification, the actual mechanism of meridional transport (e.g., eddy thickness fluxes or geostrophic flow) has no bearing on the mass balance for the box. We do, however, require that the circumpolar-mean meridional transport T^{ACC} be supported by eddy thickness fluxes:

$$\frac{1}{L_A + L_P} \sum_{i=A,P} L_i[\psi_i]_{y_{in}}^{0} = \frac{1}{L_A + L_P} \sum_{i=1}^{n} T_i^{\mathrm{ACC}} = K s_n, \qquad (7)$$

consistent with previous theory (Marshall and Radko 2003), where K is the isopycnal eddy (thickness) diffusivity. This approach allows us to circumvent the distinction between eddy thickness fluxes and meridional geostrophic flows within each sector of the ACC.

a. Box approximation of the residual-mean equations

To formalize our isopycnal box model, we first apply (6) and (7) on adjacent isopycnal surfaces to express mass conservation within each of the ACC's isopycnal boxes (see Fig. 4):

$$[(T_n^{\kappa} - T_{n-1}^{\kappa}) + (T_n^{\mathrm{ml}} - T_{n-1}^{\mathrm{ml}}) + \mathcal{S}_n]_A = -\chi_n, \qquad (8)$$

$$[(T_n^{\kappa} - T_{n-1}^{\kappa}) + (T_n^{\mathrm{ml}} - T_{n-1}^{\mathrm{ml}}) + \mathcal{S}_n]_P = \chi_n, \quad \text{and} \qquad (9)$$

$$\sum_{i=A,P} (T_{i,n}^{\kappa} - T_{i,n-1}^{\kappa}) + \mathcal{S}_{A,n}^{\mathrm{NADW}} = -T_n^{\mathrm{ACC}}. \qquad (10)$$

The diabatic transports T^{κ} and T^{ml}, defined below, represent diffusive upwelling in the northern basins and surface water mass transformation, respectively. The χ terms measure the net zonal convergence of mass between basins, which is typically much smaller than the zonal transport in a given isopycnal layer. The sign convention is that positive χ represents a convergence from the Pacific to the Atlantic. The $\mathcal{S}$ terms are sources ($\mathcal{S} > 0$) and sinks ($\mathcal{S} < 0$) related to high-latitude, deep- and bottom-water formation (T^{NADW} and T^{AABW} in Fig. 4), and T^{ACC} is isopycnal meridional transport in the ACC. We take high-latitude dense water formation rates to be external parameters of the model, both for simplicity and because it is difficult to achieve large buoyancy fluxes using a relaxation boundary condition without introducing ad hoc buoyancy distributions $\hat{b}$ that have large anomalies near the domain boundaries.

In a single-basin, or circumpolarly averaged, residual-mean model, the ACC may host an arbitrary zonal transport. With multiple basins, however, zonal mass convergence χ is permitted in each density layer that enters the ACC, as long as the depth-integrated zonal mass transport is nondivergent. Thus, the zonal transport is no longer arbitrary and additional constraints must be imposed on the system. Zonal mass conservation may be expressed as

$$\sum_n \chi + T^{\mathrm{ITF}} = 0, \qquad (11)$$

where (11) includes the contribution from zonal transport through the ITF (section 3d).[2] We also satisfy a simplified momentum budget, ostensibly arising from bottom friction, by constraining the barotropic velocities using

$$L_A U_A^{\mathrm{BT}} + L_P U_P^{\mathrm{BT}} = (L_A + L_P) U^{\mathrm{BT}}, \qquad (12)$$

where L_A and L_P are the zonal width of each sector. The mean barotropic velocity U^{BT} is a prescribed external parameter, but U_A^{BT} and U_P^{BT} are components of the model solution.

Deep-water formation in the Atlantic Basin is included in our model through the external parameter T^{NADW}, which is a transfer of mass from a lighter density layer into a heavier density layer (from $b_{A,1}$ to $b_{A,3}$ in Fig. 4). A limitation of this model is that the density classes from which NADW is removed and injected are fixed. More complicated parameterizations could be applied, especially with a view toward identifying transitions in the overturning structure. For model configurations with an explicit AABW layer (the lowermost density class), bottom-water production can also be included. In these cases, the outcrop position of the lowermost interface is pinned to the southern boundary of the domain, for example, $y_{N-1} = -\ell$ and $T_{i,N-1}^{\mathrm{ml}} = T_i^{\mathrm{AABW}}$, where $i = A, P$. The partitioning of deep-water formation between the Atlantic and Pacific Basins is prescribed. Equations (8)–(12) are solved simultaneously to arrive at the steady-state stratification and overturning. The remainder of this section provides the expressions

[2] In (8) and (9), T^{ITF} is dropped for the simplicity of the model development; however, this term is included for $n = 1$ in our model solutions.

defining the T's and χ's; model solutions are presented in section 4.

b. Diffusive upwelling

In the northern basins, vertical transport between density classes is controlled by the imposed diapycnal diffusivity and the vertical buoyancy distribution. Adapting the relationship derived in (2.12) of Nikurashin and Vallis (2011) to a model with a small number of density classes, we apply the following scaling for the diffusive transport:

$$T^{\kappa}_{i,n} = -\frac{\kappa L_i L_y}{z_n}, \tag{13}$$

where L_i is the zonal width of the sector, and L_y is the meridional length of the basin. Positive T^{κ} corresponds to an upward transport.

The diapycnal diffusivity κ may have a vertical structure, in which case (13) employs the value $\kappa(z_n)$. In section 4, we use the form

$$\kappa(z) = \kappa_0 - \Delta\kappa \tanh\left(\frac{z - d_\kappa}{\ell_\kappa}\right), \tag{14}$$

where κ_0, $\Delta\kappa$, d_κ, and ℓ_κ are constants describing a reference diffusivity, the diffusivity range, a diffusivity transition depth, and a vertical length scale associated with this transition. This vertical structure provides an idealized representation of the relatively weak diapycnal mixing rates in the upper ~2000 m of the ocean (Bryan and Lewis 1979; Ledwell et al. 1993). We assume constant L_i and L_y in each zonal sector, whereas in the ocean the horizontal surface area varies with depth; this hypsometric effect could be incorporated but is neglected here for simplicity.

c. ACC water mass modification and meridional transport

The ACC boxes of the model are adiabatic, so transformation only occurs where layer interfaces outcrop at the surface. There are various ways of introducing buoyancy forcing at the outcrop position in the surface Southern Ocean (Stewart et al. 2014). Here, the buoyancy flux B, defined at each isopycnal outcrop position and integrated from the base of the mixed layer $z = -h_m$ to the surface, is calculated based on restoring to a prescribed meridional buoyancy distribution $\hat{b}(y)$:

$$B_{i,n} = \frac{h_m}{\tau_r}[\hat{b}(y_{i,n}) - b^*_n], \tag{15}$$

where τ_r is the relaxation time scale, and $\hat{b} = b_0 \cos(\pi y/\ell)$ is taken to be zonally uniform but could be defined separately for each zonal sector. The transformation occurs at the outcrop position with $b^*_n = (b_n + b_{n+1})/2$, the buoyancy associated with the interface.

Following Marshall and Radko (2003), the transport streamfunction at the base of the mixed layer in the ACC channel is given by $B/\partial_y b_s$, where $\partial_y b_s$ is the surface meridional buoyancy gradient. With a small number of density layers, $\partial_y b_s$ is approximated by $\Delta b/\ell^{\mathrm{ml}}$, where $\Delta b_n = b_n - b_{n+1}$ and $\ell^{\mathrm{ml}}_{i,n} = (y_{i,n-1} - y_{i,n+1})/2$. The overturning transport in the mixed layer is then given by

$$T^{\mathrm{ml}}_{i,n} = \frac{B_{i,n}\ell^{\mathrm{ml}}_{i,n} L_i}{\Delta b_n}. \tag{16}$$

Positive T^{ml} represents a conversion of denser water to lighter water and an equatorward transport; for $T^{\mathrm{ml}} < 0$, the transport is poleward.

Closure of the box model also requires a parameterization of the meridional transport in the ACC. The slope of each interface is determined as part of the solution, allowing the residual transport to accommodate the diapycnal upwelling in the northern basins. Our scaling for the meridional transport follows the residual-mean theory of Marshall and Radko (2003) and Marshall and Speer (2012): meridional transport is down the isopycnal thickness gradient in a circumpolarly averaged sense. The meridional layer thickness gradient is equivalent to a difference in isopycnal slope between the upper and lower bounding surfaces of the isopycnal layer. Thus, we define the total ACC transport as

$$T^{\mathrm{ACC}}_n = -K(L_A + L_P)\Delta s_n, \tag{17}$$

where $\Delta s_n = s_{n-1} - s_n$ [see also (7) and (A12)]. In this model, we set the surface slope s_0 and the bottom slope s_N to be consistent with a fully compensated residual streamfunction ($\psi = 0$), which implies $s_0 = s_n = \tau/(\rho_0 f L)$, where τ is the surface wind stress.[3] Because T^{ACC} and s represent net circumpolar characteristics, the meridional transport does not necessarily follow a downgradient thickness flux in each ACC sector, as discussed in section 6.

d. Zonal transport

The zonal transport is composed of both barotropic and baroclinic parts. The baroclinic velocities can be defined in terms of the model parameters and s_n. We assume that the zonal velocity in the lowermost density layer is due to the barotropic component alone, and

[3] Setting surface and bottom slopes equal to zero does not qualitatively change the solution. Setting the same slope at the ocean surface and bottom results in zero depth-averaged lateral ACC transport, assuming K has no depth dependence.

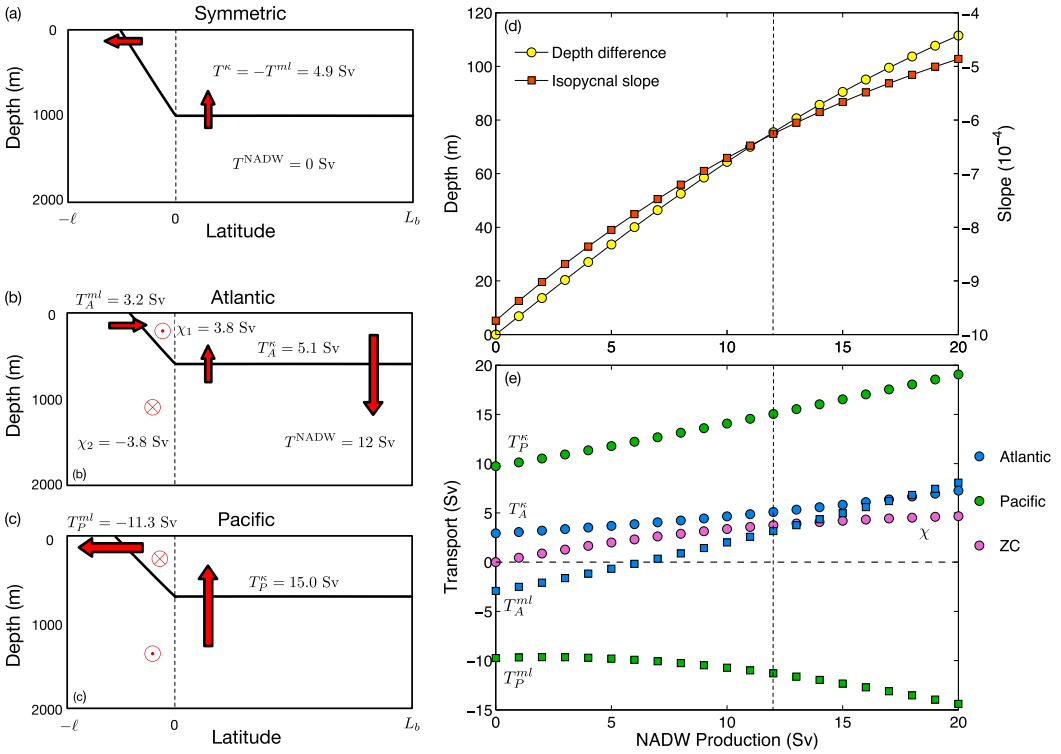

FIG. 5. Summary of a two-layer box model using parameters in Table 1. (a) Depth of the density interface for a symmetric case with $T^{\mathrm{NADW}} = 0$. Asymmetry in basin widths and NADW production modifies the transport and stratification in each basin; (b),(c) an example is provided. (d) Sensitivity of the difference in interface depth $z_{A1} - z_{P1}$ (yellow) and ACC isopycnal slope s (orange) to NADW production. (e) Transport sensitivity to NADW production; transport definitions are provided in section 3. The dashed line in (d) and (e) correspond to (b) and (c). In all experiments, the ocean depth was 3000 m.

$$U_n^{\mathrm{BC}} = \frac{\Delta b_n}{f} s_n, \quad U_N^{\mathrm{BC}} \equiv 0. \tag{18}$$

With these relationships, the transport convergence in each layer is given by the difference in the zonal transport between the two basins:

$$\chi_n = \left(U_P^{\mathrm{BT}} + \sum_{k=n}^{N-1} U_k^{\mathrm{BC}} \right) \mathcal{A}_{Pn} - \left(U_A^{\mathrm{BT}} + \sum_{k=n}^{N-1} U_k^{\mathrm{BC}} \right) \mathcal{A}_{An}, \tag{19}$$

where the values $\mathcal{A}_{i,n}$ refer to the area in the depth–meridional plane of the nth density class in the ith zonal sector.

A final component of the model is the important role of the ITF, which provides an alternative pathway for the zonal transport of mass. We assume that zonal transport across the shallow sill of the ITF arises from a balance between the zonal pressure gradient and friction. Thus, we parameterize the zonal transport based on the thickness of the uppermost density layers:

$$T^{\mathrm{ITF}} = C_{\mathrm{ITF}}(z_{A1} - z_{P1}), \tag{20}$$

where C_{ITF} is a constant with units of meters squared per second that is related to the geometry of the ITF and frictional parameters. This relationship assumes that the baroclinic compensation of the pressure gradient arising from sea surface height anomalies occurs at the depth of the first density interface. This is a rather crude approximation; however, Wyrtki (1987) and Sprintall and Révelard (2014), among others, have found a strong correlation between SSH anomalies and the strength of the ITF transport. We select C_{ITF} equal to $5 \times 10^5\,\mathrm{m^2\,s^{-1}}$ because this produces a realistic ITF strength for a isopycnal depth difference on the order of 10 m, but the solutions are not qualitatively sensitive to C_{ITF} as long as its magnitude is of $O(10^5)\,\mathrm{m^2\,s^{-1}}$.

4. The three-dimensional overturning circulation

a. *Two-layer model*

To build intuition about the box model, we first consider a two-basin, two-layer scenario (Fig. 5). AABW

TABLE 1. Box model parameters for the solutions discussed in section 4. For the two-layer example (Fig. 5), $\Delta\kappa$, d_κ, and ℓ_κ are set to zero. The parameters b_j below only apply to the four-layer experiment.

Parameter	Value	Description
L_y	10×10^6 m	Meridional basin length
ℓ	2×10^6 m	Meridional ACC length
L_A	3×10^6 m	Atlantic Basin width
L_P	10×10^6 m	Pacific Basin width
H	4000 m	Ocean depth
f	1×10^{-4} s^{-1}	Coriolis frequency
ρ_0	1000 kg m^{-3}	Reference density
b_0	6×10^{-3} m s^{-2}	Buoyancy range
b_1, b_2, b_3, b_4	$b_0 \times (1, -1/3, -3/4, -1)$	Layer densities (four-layer model)
K	1×10^3 m^2 s^{-1}	ACC isopycnal diffusivity
h_m	150 m	Mixed layer depth
τ_r	1.3×10^6 s	Mixed layer Relaxation scale
U^{BT}	0.02 m s^{-1}	Bottom (barotropic) velocity
κ_0	1×10^{-4} m^2 s^{-1}	Reference diapycnal diffusivity
$\Delta\kappa$	5×10^{-5} m^2 s^{-1}	κ range
d_κ	1800 m	κ transition depth
ℓ_κ	700 m	κ scale depth
C_{ITF}	5×10^5 m^2 s^{-1}	Indonesian Throughflow parameter

is not included, $T_{A,P}^{\mathrm{AABW}} = 0$, and the diapycnal diffusivity is constant: $\kappa = 1 \times 10^{-4}$ m^2 s^{-1}. If the basins are zonally symmetric, that is, there is no NADW formation and the basin widths are the same, the OC consists of a diffusive upwelling and a transformation to the denser buoyancy class in the Southern Ocean mixed layer (Fig. 5a). As NADW formation and asymmetric basin widths are introduced, $L_A/L_P = 0.3$, a more complex OC develops (Figs. 5b,c). Water mass modification in the mixed layer of the Southern Ocean develops opposite signs in the different basins—water becomes lighter in the Atlantic Basin (equatorward transport) and denser in the Pacific Basin (poleward transport). The Pacific can support a larger diffusive upwelling because of its larger width. Thus, nearly 4 of the 12 Sv (1 Sv $\equiv 10^6$ m^3 s^{-1}) that downwell as NADW in the Atlantic are transported zonally to the Pacific through the ACC. The zonal convergence in the upper layer, from the Pacific to the Atlantic, is accomplished by having a deeper upper layer in the Pacific as compared to the Atlantic. Thus, even in the simplest version of the box model, the differing stratification between the basins is dynamically linked to a transfer of deep and bottom waters from the Atlantic to the Pacific and its return in lighter density classes. This result is consistent with Jones and Cessi (2016).

The right-hand panels of Fig. 5 show the dependence of the upper-layer thickness difference ($z_A - z_P$), the isopycnal slope of the ACC s and the transports T to changes in NADW production. Allowing the outcrop position y_1 to be a component of the solution illustrates the link between high-latitude processes in both hemispheres. As the strength of NADW production intensifies, z_1 shoals in both sectors to generate a larger diffusive flux. This leads to a shallower slope across the ACC that reduces the mean meridional ACC transport T^{ACC} (Fig. 5e). This then requires a larger zonal exchange between the two basins to accommodate the modified water mass transformation in the Southern Ocean mixed layer. As the zonal transport increases, the difference in stratification becomes larger as well. In this two-layer model, χ reaches a maximum of 5 Sv for $T^{\mathrm{NADW}} = 20$ Sv (Fig. 5f); zonal exchange becomes a larger percentage of T^{NADW} for a greater number of layers, as shown below. In Fig. 5d, the difference in interface depth is roughly 50 to 100 m. This value is smaller than the observed difference in isopycnal heights across basins. However, we show in section 5 that this discrepancy can be explained by our assumption of a constant slope across the ACC.

b. *Four-layer model*

To represent all of the major water masses that participate in the OC, a model with at least four layers is required. An example solution with a four-layer stratification is shown in Fig. 6. From top to bottom the layers can be thought of as Intermediate Water, Upper Circumpolar Deep Water (UCDW), Lower Circumpolar Deep Water (LCDW) or NADW, and AABW. We prescribe that the formation of AABW occurs exclusively in the Atlantic Basin. The outcropping y_3 is fixed at the southern boundary in each basin, but y_1 and y_2 are part of the model solution. In this solution, the interface separating LCDW from AABW is about 150 m deeper in the Pacific than the Atlantic.

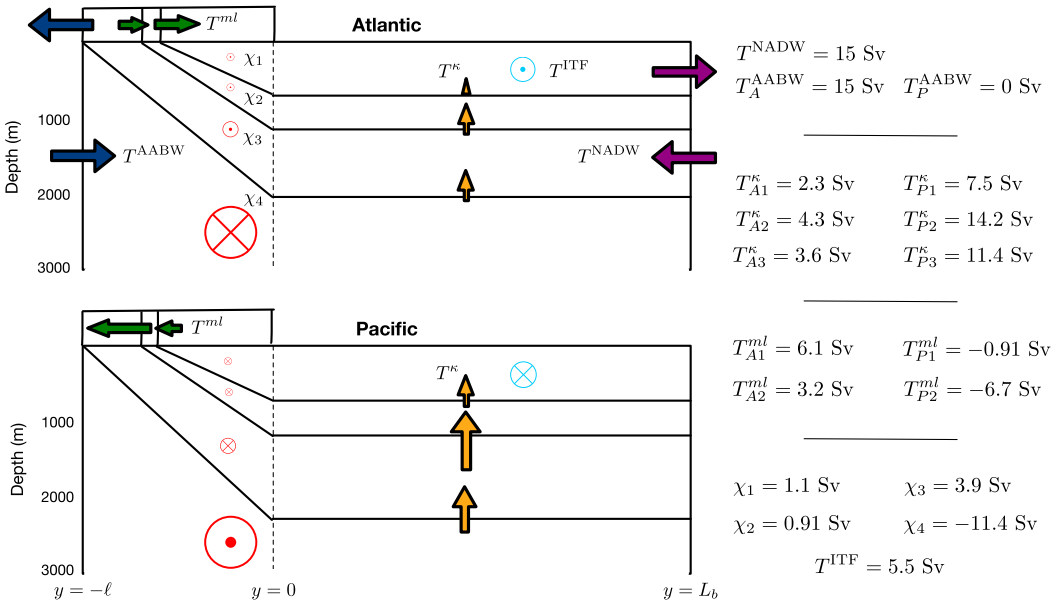

FIG. 6. Example stratification, transport T, and zonal convergence χ in a four-layer, two-basin box model. Conceptually the layers correspond to Intermediate Water, Upper Circumpolar Deep Water, Lower Circumpolar Deep Water (NADW), and Antarctic Bottom Water density classes; the full ocean depth is 4000 m. Solid lines indicate the interfaces between these layers in each basin. Transports (Sv) are given to the right of the schematic. Positive values of χ indicate transport from the (bottom) Pacific to the (top) Atlantic. See Fig. 4 for further information about transports.

The key result of Fig. 6 is the zonal transport of 11.5 Sv from the Atlantic to the Pacific in the lowermost density class. This accounts for approximately 75% of the downwelled NADW. Additionally, the return flow to the lightest density class in the Atlantic, or the site of NADW formation, is partitioned between three components: diffusive upwelling (2.3 Sv), formation of Intermediate Water (7.2 Sv), and transport through the ITF (5.5 Sv). The contribution from the ITF is remarkably strong and is a robust feature of the model for realistic parameters. The ITF provides a pathway of zonal exchange for the lightest density classes. This pathway may be favored because of the difficulty in generating zonal convergence in the ACC in shallow layers that have a relatively small areal extent. In general, χ_1 and χ_2 tend to be much smaller than χ_3 and χ_4 in these solutions.

The sensitivity of the four-layer model to changes in the strength of NADW formation (Figs. 7a,b) has similarities to the two-layer model results in Fig. 5. As T^{NADW} increases in magnitude, the interface between NADW and AABW shoals, with this interface being approximately 200 m deeper in the Pacific Basin. The ACC isopycnal slopes also shoal (not shown), which influences the outcropping position. An increase in T^{NADW} results in an increase in T^{ITF}, which was not included in the two-layer example (Fig. 7b). The zonal exchange of mass in the lowest density class is insensitive to changes in T^{NADW}, since T^{AABW} is prescribed in this simulation (Fig. 7b). However, as T^{NADW} strengthens, more of the zonal transport into the Atlantic occurs through the ITF, until the transport through the ITF dominates the interbasin exchange for $T^{\mathrm{NADW}} = 20$ Sv. Diffusive upwelling is enhanced in the Pacific because of the basin's larger width. Although it is important to keep in mind that the ratio $T_{A3}^{\kappa}/T_{P3}^{\kappa} > L_A/L_P$, which is consistent with a thinner LCDW layer in the Atlantic and the parameterization (13). The ratio of the diffusive transports in each basin is relatively insensitive to T^{NADW} in these uniform slope simulations.

Water mass transformation occurring at the surface of the Southern Ocean may be influenced by the relative basin widths (Fig. 7c). For a narrow Atlantic Basin, the transport is equatorward across y_1 and y_2, indicating a positive buoyancy flux and the formation of Intermediate Waters. However, as the basin widths become comparable, the outcropping sites are pushed further to the south, and the buoyancy forcing changes sign across the interface separating upper and lower CDW y_2. Tamsitt et al. (2016) have recently shown that positive heat fluxes are more prominent in the Atlantic sector of the ACC, as compared to the Pacific sector. This box model suggests that at least part of this zonal asymmetry can be attributed to the narrow width of the

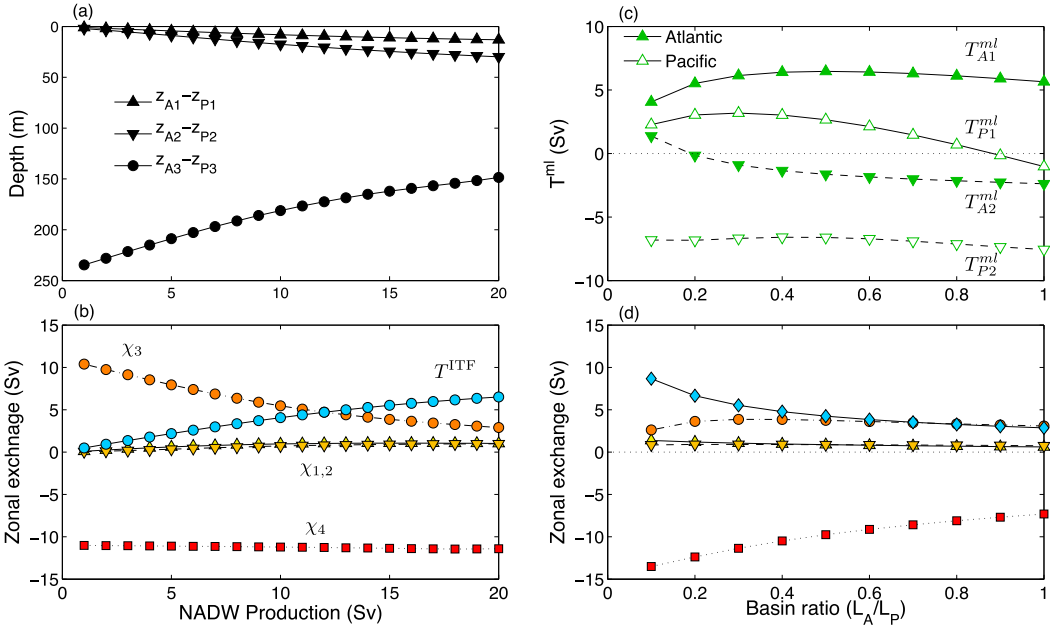

FIG. 7. Sensitivity of the four-layer box model to (left) NADW production rates and (right) the basin width ratio L_A/L_P. (a) Difference in layer interface as a function of T^{NADW}; positive values indicate that the Pacific is deeper than the Atlantic. (b) Sensitivity of the strength of surface ACC transformation T^{ml} to the basin width ratio. Sensitivity of the zonal exchange, including T^{ITF} in different density classes to (c) T^{NADW} and (d) L_A/L_P. Parameters held fixed are given in Table 1. Symbols are the same in (c) and (d).

Atlantic Basin. Similar spatial patterns are apparent in the distribution of the Southern Ocean water mass subduction (Sallée et al. 2012). Zonal transport of AABW between basins occurs regardless of the basin width (Fig. 7d), although overall the zonal exchange is reduced as the basin widths become of comparable size. Note that asymmetry still arises due to T^{NADW} and T^{AABW}. For this set of parameters, we find that the return from the Pacific to the Atlantic is almost equally partitioned between χ_3 and T^{ITF} when $L_A = L_P$.

So far, we have prescribed a transformation of NADW into AABW exclusively in the Atlantic sector of our box model, reflecting the predominance of AABW generated in the Weddell Sea. However, AABW forms at a number of sites around the Antarctic margins (Jacobs et al. 1970; Aoki et al. 2005; Ohshima et al. 2013). Zonal exchange in the ACC, which is largely confined to layers $n = 3, 4$, is more sensitive to changes in T_A^{AABW} than to T_P^{AABW} (Fig. 8). The zonal exchange in these layers may acquire both positive and negative values for the range of parameters explored here. Weak values of T_A^{AABW} are associated with a transport of mass from the Atlantic to the Pacific in the LCDW density class. The zonal exchange through the ITF (Fig. 8c) has a more complicated dependence on bottom-water formation rates, although the range of variability is relatively small; T^{ITF} depends more sensitively on NADW formation rates. Future iterations of this model should allow for internal feedback between model stratification, buoyancy forcing, and deep/bottom-water formation rates.

c. *Overturning transitions*

A motivation for exploring a three-dimensional OC is to recover transitions in the overturning structure. Ferrari et al. (2014) argued that the transition from a "two-cell" to a figure-eight circulation structure between the LGM and the present was related to a shoaling of NADW above the Mid-Atlantic Ridge. They indicate that this shift necessarily accompanies changes in sea ice extent. Figure 9 shows that a rapid transition in overturning structure may occur because of modifications in other external parameters. The solution to a four-layer model is shown, where T^{NADW} is updated so that water is removed from layer $n = 1$ and injected into layer $n = 2$, rather than $n = 3$. This allows for the possibility of a purely diffusive AABW cell in the two densest layers. The diagnostic plotted in Fig. 9, $r = |T^{\mathrm{ml}}_{A1}/T^{\mathrm{ml}}_{A2}|$, describes the ratio of NADW, upwelled into the mixed layer of the ACC, that is converted into lighter Intermediate Waters T^{ml}_{A1} and denser Bottom Waters T^{ml}_{A2}. Grossly, $r < 1$ and $r > 1$ correspond to overturning structures that are more figure-eight-like and more two-cell-like, respectively. For a uniform

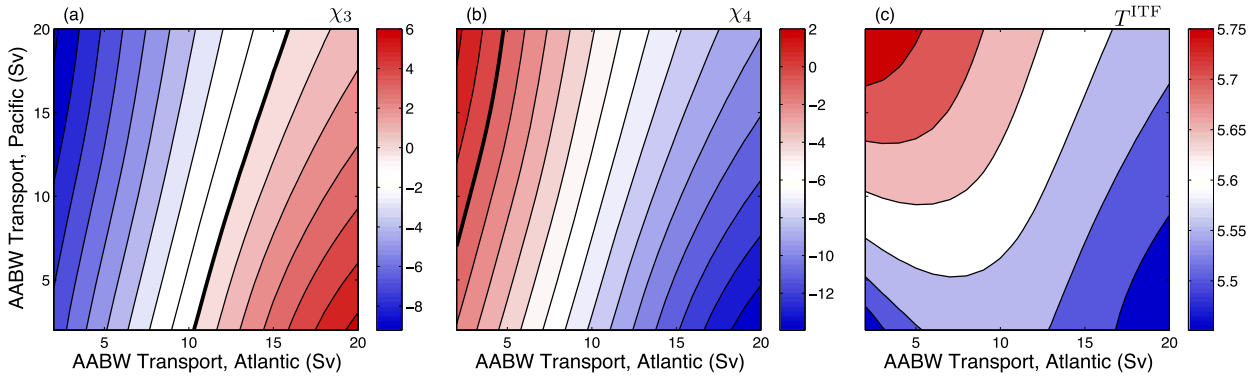

FIG. 8. Sensitivity of zonal exchange terms (a) χ_3, (b) χ_4, and (c) T^{ITF} to changes in AABW formation rates (Sv) in both Atlantic and Pacific Basins. Note the change in contour interval in each panel. The solid curves in (a) and (b) mark the 0-Sv contour.

diapycnal diffusivity (blue curves), increasing NADW production shoals the stratification and leads to a progressively stronger adiabatic, upper overturning cell as the surface buoyancy forcing in the ACC intensifies. However, in a situation where there is sharp transition in the intensity of diffusive upwelling (red curves), the upper, adiabatic overturning cell is initiated abruptly as the interface z_2, separating NADW and AABW, crosses this threshold. NADW and AABW are effectively isolated at this point, as has been argued to be the case at the LGM (Curry and Oppo 2005; Lund et al. 2011; Ferrari et al. 2014). The magnitude of the overturning here is less important than the relative change because of the idealized nature of the model. Critically, though, a transition with this behavior cannot be captured in a single-basin model.

5. Why are isopycnals so much deeper in the Atlantic than the Indo-Pacific?

In the previous section, a three-dimensional OC is shown to predict a deeper stratification in the Pacific as compared to the Atlantic, but the magnitude of this difference is smaller than observed in the ocean. Figure 3c suggests that this is because the separation of the Atlantic and Indo-Pacific isopycnal depths occurs close to the northern edge of the ACC, whereas in our box model the isopycnals are uniformly separated in the ACC. For the same zonal convergence/divergence, isopycnals that diverge only at the northern edge of the basin can achieve a larger separation distance. In this section, we pose an explanation for the observed shapes of the Atlantic versus Indo-Pacific isopycnals in the

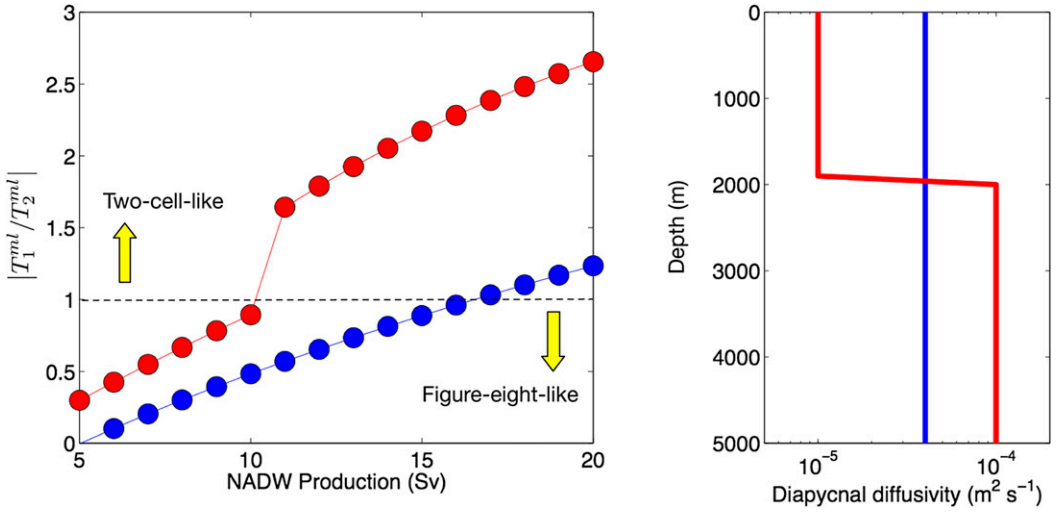

FIG. 9. (a) Ratio of NADW water mass conversion into Intermediate Water T_{A1}^{ml} and into denser Bottom Water T_{A2}^{ml} as a function of NADW production for both uniform background diffusivity (blue) and for diffusivity with an abrupt vertical transition (red). (b) Vertical diffusivity profiles, $\kappa(z)$ for each case.

ACC by returning to the general, two-basin, residual-mean equation (5).

As above, the ACC is a channel of meridional width l with northern boundary at $y = 0$ and southern boundary at $y = -l$. The ACC is divided into two sectors, Atlantic and Pacific, with zonal lengths L_A and L_P and sector-mean isopycnal depths $z_A(y)$ and $z_P(y)$, respectively. To obtain an analytically tractable model, we begin with (5) and make the following simplifications:

(i) We seek a steady solution: $\partial z_{A,P}/\partial t = 0$.
(ii) We neglect diapycnal mixing κ and direct buoyancy forcing B in the ocean interior, assuming perfectly adiabatic transport.
(iii) We assume that the zonal wind stress and the lateral eddy diffusivity are both zonally and meridionally invariant and denote them as τ and K, respectively, in both basins.
(iv) We assume that the velocity can be written as a simple linear vertical shear

$$u \approx U + U_z z \Rightarrow \Psi_i \approx -U z_i - \frac{1}{2} U_z z_i^2, \qquad (21)$$

where U and U_z are constants and $i = A, P$. This assumption requires that the interbasin change in the isopycnal slope is small relative to the mean isopycnal slope.
(v) We assume that the meridional streamfunction ψ is dominated by its wind- and eddy-driven components and that the geostrophic component [the last term on the right-hand side of (A15)] may be neglected:

$$\psi_i \approx -\frac{\tau}{\rho_0 f} + K\frac{\partial z_i}{\partial y}. \qquad (22)$$

This assumption is valid, for example, if interbasin anomalies in isopycnal depth are confined over a relatively short meridional length scale, as suggested by Fig. 3, and confirmed in our solution below.

These assumptions reduce (5) to a coupled pair of linear ordinary differential equations for the isopycnal depths in the Atlantic and Pacific sectors:

$$\frac{d}{dy}\left(-\frac{\tau}{\rho_0 f} + K\frac{dz_A}{dy}\right) = \frac{U}{L_A}(z_A - z_P) + \frac{(1/2)U_z}{L_A}(z_A^2 - z_P^2), \qquad (23a)$$

and

$$\frac{d}{dy}\left(-\frac{\tau}{\rho_0 f} + K\frac{dz_P}{dy}\right) = \frac{U}{L_P}(z_P - z_A) + \frac{(1/2)U_z}{L_P}(z_P^2 - z_A^2). \qquad (23b)$$

The left-hand side of each of these equations resembles the adiabatic residual-mean equations of Marshall and Radko (2003). The right-hand side comprises the additional contribution due to convergence/divergence of mass above/below isopycnals due to differences in the Atlantic and Pacific isopycnal depths.

Equations (23a) and (23b) apply, under assumptions i–v, to any isopycnal that exists in both the Atlantic and Pacific sectors. However, we will restrict our attention to the isopycnal that separates the northward- and southward-flowing branches of the OC in the Southern Ocean. Ferrari et al. (2014) identify this isopycnal with the $27.9\,\mathrm{kg\,m^{-3}}$ neutral density surface, which reaches the surface approximately at the annual-mean sea ice edge. This isopycnal does not quite outcrop at the ocean surface (see Fig. 3) but instead flattens out at the southern edge of the ACC or at $y = -l$ in our notation. We suppose that there is a net sinking of waters T (measured in cubic meters per second) across this isopycnal in the North Atlantic and that all of this water ultimately upwells diffusively in the Pacific Basin. The circumpolar-averaged residual streamfunction is therefore zero at the northern edge of the ACC:

$$\psi_A = T/L_A, \quad \psi_P = -T/L_P \quad \text{at} \quad y = 0. \qquad (24)$$

As there is no interbasin exchange south of the ACC, it also follows that both the Atlantic and Pacific overturning streamfunctions must vanish at $y = -l$:

$$\psi_A = \psi_P = 0 \quad \text{at} \quad y = -l. \qquad (25)$$

This scenario is illustrated schematically in Fig. 2, though in this section we neglect the role of the ITF for simplicity.

The solution of (23a)–(25) is described in appendix B. For analytical convenience, we pose this solution using alternative variables:

$$\zeta = \frac{L_A z_A + L_P z_P}{L_A + L_P}, \quad \text{and} \quad \Delta = z_A - z_P, \qquad (26)$$

where ζ is the circumpolar-averaged isopycnal depth, and Δ is the difference between the isopycnal depths in the Atlantic and Pacific sectors. The complete solution is given in terms of Airy functions by (B4) and (B12) and yields little intuition when written out in full. To aid the interpretation of the solution, in appendix B we show that by additionally assuming that the change in zonal velocity across the isopycnal is small, $Us/U_z l \ll 1$, the solution may be approximately written as

$$\zeta = \zeta|_{y=0} + \frac{\tau}{\rho_0 f K} y, \quad \text{and} \qquad (27a)$$

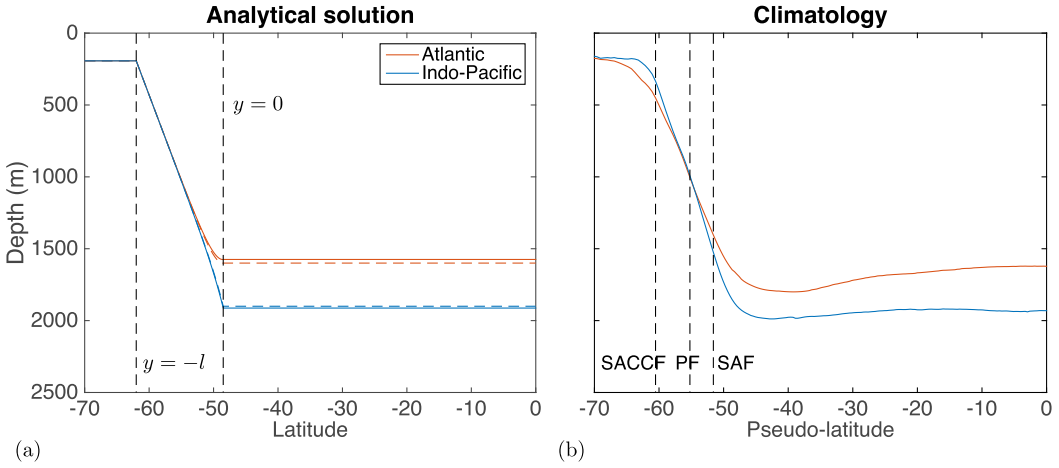

FIG. 10. Zonal-mean isopycnal depths in the Atlantic and Pacific (Indo-Pacific), as predicted by (a) our analytical solution from section 5 and (b) the along-stream-averaged 27.9 kg m^{-3} neutral density surface from Fig. 3. In (a), the solid lines correspond to the full analytical solution, given by (B4) and (B12), while the dashed lines correspond to the approximate solution given by (27a)–(27b). Our solution predicts that isopycnals should lie shallower in the Atlantic sector than in the Pacific in order to support zonal convergence/divergence of mass between basins and thus complete the figure-eight global OC. The balance between this zonal convergence/divergence and the corresponding meridional divergence/convergence of mass within isopycnal layers by eddy thickness fluxes implies that the isopycnal depth difference should be concentrated close to the northern edge of the ACC. Model parameters are given in section 5.

$$\Delta \approx \frac{T\Lambda}{K}\left(\frac{1}{L_A}+\frac{1}{L_P}\right)e^{y/\Lambda}. \tag{27b}$$

Here, the diffusive length scale Λ is given as

$$\Lambda = \sqrt{\frac{K/U}{1/L_A + 1/L_P}}. \tag{28}$$

For typical parameter values, $\Lambda \approx 200$ km, which is much smaller than the width of the ACC: $\Lambda/\ell \ll 1$ (see appendix B). The form of (27b) suggests that the isopycnal depth difference Δ is effectively zero outside of a narrow, meridional boundary layer of width $O(\Lambda)$ at the northern edge of the ACC, consistent with the along-stream-averaged isopycnal depths shown in Fig. 3.

In Fig. 10, we compare the full analytical solution, (B4) and (B12), against the climatological 27.9 kg m^{-3} neutral density surface from Fig. 3. In both panels, the Atlantic and Pacific isopycnals lie at approximately the same depth across most of the ACC but then separate close to the northern boundary such that the isopycnal lies shallower in the Atlantic. To produce Fig. 10a, we chose an ACC width of $l = 1500$ km and assigned the lengths of the Atlantic and Indo-Pacific based on the longitude ranges shown in Fig. 3b, using the mean latitude of the Polar Front (~55°S) to calculate zonal distances in units of meters. We chose the isopycnal depth at the northern edge of the ACC to be $\zeta_{y=-1} = -1800$ m, approximately equal to the circumpolar-mean depth of the 27.9 kg m^{-3} neutral density surface. We chose typical scales for $\rho_0 = 1000$ kg m^{-3} and $f = -10^{-4}$ rad s^{-1}. We set the zonal velocity maximum to $U = 0.15$ m s^{-1} and chose U_z such that the zonal velocity vanished at $z = -4000$ m. The isopycnal depth difference at the northern edge of the ACC is sensitive to the various parameters in (29), so we selected the parameter combination $K = 1400$ m^2 s^{-1}, $\tau = 0.15$ N m^{-2}, and $T = 8$ Sv, which yields good visual agreement between the analytical solution and the climatology. However, none of these parameters are particularly well constrained, and many simplifications have been made to obtain this analytical solution.

Equation (27b) immediately yields a scaling for the isopycnal depth difference at the northern edge of the ACC:

$$\Delta|_{y=0} \approx \frac{T\Lambda}{K}\left(\frac{1}{L_A}+\frac{1}{L_P}\right). \tag{29}$$

Using the parameter values described above, we obtain $\Delta|_{y=0} \approx 300$ m. Crucially, (29) does not depend on the width of the ACC because the interbasin transport occurs within the meridional boundary layer of width $O(\Lambda)$. A naive scaling derived under the assumption of linear isopycnals in each sector of the ACC would conclude that the isopycnal depth difference should scale as $\Delta \sim T/Ul$. For the same parameter values as above, this predicts an isopycnal depth difference of only $\Delta \approx 36$ m, comparable to the box model solutions but much smaller than observed.

This suggests the reason the Atlantic middepth isopycnals lie several hundred meters higher than their counterparts in the Pacific may be because the interbasin transport is concentrated at the northern edge of the ACC.

Finally, we emphasize that we do not claim that eddy bolus transport convergence is solely responsible for the large change in isopycnal depth between the Atlantic and Pacific: rather, the spread of the isopycnals close to the northern edge of the ACC may also permit meridional geostrophic flows in the ACC that facilitate interbasin convergence/divergence of mass above/below isopycnals (Jones and Cessi 2016). We explicitly neglected geostrophic meridional flows here, but we emphasize that both mechanisms may be at work in the real ACC, combining to produce the observed interbasin differences in isopycnal depths.

6. Discussion

Reid's (1961) description of the differing physical characteristics of the ocean basins (see Fig. 1) preceded dynamical models of the OC. It is rather remarkable that most conceptual models of the OC are unable to reproduce these fundamental characteristics of the modern ocean. Simplifying assumptions have always guided conceptual models of the overturning circulation (e.g., Munk 1966; Marshall and Radko 2003). Our model introduces new degrees of freedom by adding separate basins and sectors of the ACC, which must, in turn, be justified by new insight.

The main insight gained from introducing two separate basins is the elucidation of three-dimensional water mass pathways in the global circulation. The focus in recent years on controls over the meridional OC (MOC), or sometimes just the Atlantic MOC (AMOC), has led to an established view of the overturning summarized in Fig. 2a. Zonally averaged, the overturning is typically discussed in terms of two separate cells with different dynamical balances. The strength of the lower overturning cell arises from a competition between deep-water formation around the margins of Antarctica and diffusive upwelling distributed throughout the ocean basins. The upper overturning cell, characterized by isopycnal outcropping at both high northern and southern latitudes, has the ability to form a closed loop in the absence of interior, diapycnal mixing and is often referred to as an adiabatic cell. This closed adiabatic cell implies that the two high-latitude transformation sites have buoyancy forcing of equal magnitude but of opposite sign.

This study was motivated, in part, by the hypothesis that most NADW upwells not in regions of surface buoyancy input in the ACC, but rather under the (austral summertime) sea ice edge (Ferrari et al. 2014). While underice buoyancy fluxes are poorly constrained, the absence of strong lateral buoyancy gradients under ice (Orsi and Whitworth 2005; see also Fig. 10) suggests that upwelled NADW is carried toward the Antarctic coast, where it is subsequently converted to AABW and downwells. Consequently, closing the overturning loop in the modern-day ocean cannot occur through surface processes alone. Instead, NADW is ultimately transformed (upwelled) into lighter density classes, in the northern basins. This diffusive modification preferentially occurs in the Pacific because this basin has a greater surface area and, assuming that topographic roughness does not vary significantly between basins, can host a larger upwelling. The absence of deep-water formation in the North Pacific also allows upwelling to shallower depths, which impacts outcrop locations at the surface of the ACC. It follows that a complete circuit of the overturning circulation must, at some point, be limited by diapycnal mixing, in some ways validating Munk's abyssal recipes approach.

The sensitivity of the overturning to surface boundary conditions has been discussed by Abernathey et al. (2011), Nikurashin and Vallis (2011), Stewart et al. (2014), and others. Radko and Marshall (2006) appreciated that zonal variations in this surface buoyancy flux could locally influence the strength of overturning, but recent studies have shown that transitions in the surface buoyancy flux may be more abrupt than a simple sinusoid with the gravest wavenumber (Cerovečki et al. 2011; Bishop et al. 2016). In particular, Tamsitt et al. (2016) show that while there is a large discrepancy in the surface heat flux across different basins, the intrabasin heat flux is largely uniform. This result is consistent with the models derived here in that modifications to the surface buoyancy flux are largely related to changes in the outcrop position across different basins to accommodate zonal convergence/divergence in the ACC.

The focus on the surface buoyancy forcing in the Southern Ocean raises an important point: regardless of the mechanism, either Ekman transport or eddy transport, if the overturning circulation is assumed to be in steady state, then the surface transport of water masses must be consistent with the implied water mass modification via the surface buoyancy forcing (Marshall 1997). In other words, in regions where westerly winds generate an equatorward Ekman transport that dominates the eddy component, a feature found to be nearly ubiquitous in a $1/10^\circ$ coupled climate model by Dufour et al. (2015), the surface forcing should have a tendency to make fluid in the mixed layer more buoyant.

The inclusion of the ITF in this model suggests interesting teleconnections between high-latitude deep- and bottom-water formation, zonal transport in the ACC, and

surface exchange in the Pacific/Indian Oceans. For the experiments considered in section 4, for situations where T_{NADW} is varied, but T_{AABW} is held fixed, T^{ITF} must partially accommodate changes in the high-latitude formation rates.

Our parameterization of the ACC transport as a downgradient thickness flux is consistent with isopycnal mixing of potential vorticity (Marshall and Speer 2012), and the meridional transport principally arising from eddy thickness fluxes. However, Mazloff et al. (2013) have shown that the circumpolar-mean residual meridional flow in the ACC has a substantial geostrophic component, supported by surface and topographic isopycnal outcropping. More work is needed to determine the extent to which the residual circulation of the ACC can be modeled as an eddy thickness flux.

The issues surrounding the neglect of geostrophic meridional flows are likely to be most acute in the abyssal ocean, below the depth of the ACC's major topographic features. Topographic ridges may support strong meridional geostrophic flows confined to narrow western boundary currents (Fukamachi et al. 2010). We acknowledge that this aspect of the model needs to be explored further. There are existing ad hoc methods in the literature for dealing with this complication, such as linearly reducing the meridional transport at the sill depth to zero at the bottom regardless of the density structure (Ito and Marshall 2008; Burke et al. 2015). Here, the problem is partially alleviated by our prescription of the AABW streamfunction, which implies that the lateral transport in the southern ACC is insensitive to the isopycnal slope and simply needs to balance the water mass formation rate.

A major departure between the analytical derivation in section 5 and the box model development in section 3 is the assumption of a linear, zonally uniform slope in the ACC. As shown in section 5, much of the separation between the depths of density surfaces between basins comes from curvature in these isopycnal at the northern boundary of the ACC. The box model can be modified to accommodate this curvature based on the scalings outlined in section 5, for instance by offsetting the isopycnals at $y = 0$ by Δ as defined in (29). Future uses of this model that include tracers, for instance, will need to represent the basin difference with improved fidelity to reproduce observations.

7. Conclusions

The derivation of a multibasin, residual-mean model provides a dynamical representation of a global overturning circulation that involves zonal mass transport between basins via the ACC, or via the ITF, and allows for different patterns of Southern Ocean surface buoyancy in each zonal sector. These properties are necessary to qualitatively reproduce the asymmetric water mass distributions illustrated in Fig. 1.

In section 3, the residual-mean model is idealized to a two-basin box model with linear, isopycnal slopes in the ACC, which is essentially a coarse discretization of (5). The model produces differences in both stratification and diffusive upwelling in the deep basins and differences in surface buoyancy forcing, or water mass transformation, at the surface of the Southern Ocean. The zonal exchange between basins is largest in the deepest density class, where bottom waters are exchanged from the Atlantic to the Pacific because the Pacific offers a larger horizontal area to support diffusive upwelling. Thus, when NADW reaches the surface of the ACC, it is preferentially transformed into AABW and upwelled in the Pacific, rather than being directly converted to Intermediate Waters by buoyancy input at the surface of the ACC. In section 5, we provide an analytical solution of the isopycnal slopes in the ACC balanced by convective downwelling in the North Atlantic and diffusive upwelling in the Pacific. This solution qualitatively reproduces the observed differences in isopycnal depths between the Pacific and Atlantic Basins. Again, shallower isopycnals in the Atlantic produce a convergence of deeper waters into, and a divergence of shallower waters out of, the Pacific sector of the ACC. The meridional eddy thickness fluxes constrain the interbasin exchange to a narrow [$O(200)$ km] boundary layer at the northern edge of the ACC. Consequently, the Atlantic and Pacific isopycnals diverge from one another close to the northern edge of the ACC (see Fig. 10).

These results imply a minimal role for a closed adiabatic overturning cell in the Atlantic alone. An overturning loop that cycles through both basins has implications for Lagrangian water mass pathways, ocean residence times, global tracer distributions, and transitions in the overturning structure in response to a changing climate.

Acknowledgments. We acknowledge helpful discussions with Jess Adkins, Paola Cessi, Raffaele Ferrari, Malte Jansen, C. Spencer Jones, John Marshall, Louis-Phillipe Nadeau, and Lynne Talley. AFT gratefully acknowledges support from NSF Grant OCE-1235488. ALS acknowledges support from NSF Grant OCE-1538702.

APPENDIX A

Multibasin Residual-Mean Theory in Isopycnal Coordinates

In this appendix, we derive a basin-averaged form of the conventional, three-dimensional, residual-mean

buoyancy equation [(1)] in isopycnal coordinates. Each component of the residual streamfunction can be written as a sum of mean and eddy components (e.g., Radko and Marshall 2006):

$$\psi^{(x)} = \overline{\psi}^{(x)} + \psi^{\star(x)}, \quad \psi^{(y)} = \overline{\psi}^{(y)} + \psi^{\star(y)}, \tag{A1}$$

where the mean streamfunction $\overline{\boldsymbol{\psi}} = [\overline{\psi}^{(x)}, \overline{\psi}^{(y)}]$ and eddy streamfunction $\boldsymbol{\psi}^{\star} = [\psi^{\star(x)}, \psi^{\star(y)}]$ determine the mean velocity and eddy velocity vectors, respectively, via relations analogous to (2). The mean streamfunction is simply defined as the depth integral of the mean horizontal velocity

$$\overline{\psi}^{(x)} = \int_z^0 \overline{u}\, dz, \quad \overline{\psi}^{(y)} = \int_z^0 \overline{v}\, dz, \tag{A2}$$

whereas the eddy streamfunction is proportional to the lateral eddy buoyancy flux and approximates eddy thickness transport within isopycnal layers:

$$\psi^{\star(x)} = \frac{\overline{u'b'}}{\overline{b}_z}, \quad \psi^{\star(y)} = \frac{\overline{v'b'}}{\overline{b}_z}. \tag{A3}$$

These equations constitute the standard, temporal, residual-mean approximation of the mass transport within isopycnal layers (McIntosh and McDougall 1996; McDougall and McIntosh 2001). To close the mean buoyancy equation (1), we apply a standard downgradient closure for the lateral eddy buoyancy fluxes (Gent and McWilliams 1990):

$$\overline{u'b'} = -K^{(x)}\frac{\partial \overline{b}}{\partial x}, \quad \overline{v'b'} = -K^{(y)}\frac{\partial \overline{b}}{\partial y}, \tag{A4}$$

where $K^{(x)}$ and $K^{(y)}$ are the zonal and meridional eddy buoyancy diffusivities, respectively.

We now transform to an isopycnal coordinate system, in which the mean buoyancy $\overline{b}$ is the vertical coordinate, by writing $z = z(x, y, \overline{b}, t)$. In applying the coordinate transformation, we make use of the following identities:

$$\frac{\partial f}{\partial z} = \left(\frac{\partial z}{\partial \overline{b}}\right)^{-1}\frac{\partial f}{\partial \overline{b}}, \tag{A5a}$$

$$\left.\frac{\partial f}{\partial x_i}\right|_{\overline{b}} = \left.\frac{\partial f}{\partial x_i}\right|_{z} + \frac{\partial f}{\partial z}\left.\frac{\partial z}{\partial x_i}\right|_{\overline{b}}, \quad \text{and} \tag{A5b}$$

$$\frac{\partial \overline{b}}{\partial x_i} = -\frac{\partial \overline{b}}{\partial z}\frac{\partial z}{\partial x_i}, \tag{A5c}$$

where $f(x, y, z, t) = f[x, y, z(x, y, \overline{b}, t), t]$ is an arbitrary function of space and time, and $x_i = (x, y, t)$ is any nonvertical coordinate. To rewrite the buoyancy equation [(1)] in isopycnal coordinates, we divide by $\partial\overline{b}/\partial t$, apply identities (A5a)–(A5c), and rearrange to obtain

$$\frac{\partial z}{\partial t} - \left.\frac{\partial \psi^{(x)}}{\partial x}\right|_{\overline{b}} - \left.\frac{\partial \psi^{(y)}}{\partial y}\right|_{\overline{b}} = -\frac{\partial}{\partial \overline{b}}\left[\kappa\left(\frac{\partial z}{\partial \overline{b}}\right)^{-1} + B\right]. \tag{A6}$$

Here, the subscript $\overline{b}$ indicates that horizontal derivatives of the streamfunction should be taken at constant $\overline{b}$.

Finally, we take a zonal average of (3) across a sector of the ACC of zonal length L_x. We denote the zonal average as $\langle\cdot\rangle = (1/L_x)\int_W^E \cdot\, dx$, where the limits W and E indicate the western and eastern boundaries of the sector, though this should be interpreted more generally as an average along ACC streamlines. Note that we retain a quasi-Cartesian coordinate system for simplicity, though for sufficiently convoluted streamlines this approximation becomes questionable. This yields

$$\frac{\partial\langle z\rangle}{\partial t} - \frac{1}{L_x}[\psi^{(x)}]_W^E - \frac{\partial\langle\psi^{(y)}\rangle}{\partial y} = -\frac{\partial}{\partial \overline{b}}\left[\left\langle\kappa\left(\frac{\partial z}{\partial \overline{b}}\right)^{-1}\right\rangle + \langle B\rangle\right]. \tag{A7}$$

This is the most general form of the sector-averaged, residual-mean equation in buoyancy coordinates. We now make few simplifying assumptions and notational adjustments:

(i) We neglect $\psi^{\star(x)}$ in favor of $\overline{\psi}^{(x)}$, assuming that the zonal-mean flow is much larger than the zonal eddy bolus transport.
(ii) We assume that the isopycnal depth varies slowly along streamlines in each sector, that is, $\partial z/\partial x \approx 0$ and $\langle z\rangle \approx z$ (see Fig. 3).
(iii) We simplify our notation by writing $\overline{\psi}^{(x)}$ as Ψ, $\langle\psi^{(y)}\rangle$ as ψ, $\langle K^{(y)}\rangle$ as K, $\langle\kappa\rangle$ as κ, $\overline{b}$ as b, and $\langle B\rangle$ as B.

Applying these assumptions and simplifications yields

$$\frac{\partial z}{\partial t} - \frac{1}{L_x}[\Psi]_W^E - \frac{\partial \psi}{\partial y} = -\frac{\partial}{\partial b}\left[\kappa\left(\frac{\partial z}{\partial b}\right)^{-1} + B\right]. \tag{A8}$$

The zonal streamfunction Ψ is simply equal to the vertical integral of the mean zonal velocity, as in (A2), which in turn is determined by thermal wind balance. In buoyancy coordinates these relationships may be written as

$$\Psi = -\int_{b_{\text{bot}}}^{b} \overline{u}\frac{\partial z}{\partial b}db, \quad \overline{u} = \overline{u}_{\text{BT}} + \int_{b_{\text{bot}}}^{b}\frac{1}{f}\frac{\partial z}{\partial y}db, \tag{A9}$$

where b_{bot} is the buoyancy at the ocean bottom, and $\overline{u}_{\text{BT}}$ is the barotropic velocity. The meridional streamfunction ψ follows immediately from (A1):

$$\psi = \overline{\psi} + \psi^{\star}. \tag{A10}$$

The mean component is given as

$$\overline{\psi} = -\frac{\tau}{\rho_0 f} + \frac{1}{\rho_0 f L_x}\int_z^0 [\overline{p}]_W^E \, dz', \tag{A11}$$

where $\overline{p}$ is the mean pressure, and z' is a dummy variable of integration, and the eddy component is

$$\psi^{\star} = K\frac{\partial z}{\partial y}. \tag{A12}$$

The derivation of these quantities follows Marshall and Radko (2003), except in (A11) the mean streamfunction retains a component due to the mean zonal pressure difference along the length of the ACC sector. The mean dynamic pressure may be approximated using hydrostatic balance:

$$\overline{p} = \overline{p}_0 + \int_0^z \rho_0 \overline{b}\, dz', \tag{A13}$$

where $\overline{p}$ is the surface pressure under a rigid-lid approximation.

To make use of (A8)–(A13) to describe the connectivity between basins via the ACC, we require an equation for the mean zonal transport streamfunction Ψ. To address the most general case, we consider an ACC divided into N sectors in which the variables are denoted by a subscript i for $i = 1, \ldots, N$. Then, assuming that the ACC flows eastward everywhere, we apply an upwind approximation (a concept borrowed from finite-volume discretizations of partial differential equations; e.g., LeVeque 2002) to determine the mean zonal transport streamfunction Ψ and mean pressure $\overline{p}$ on the eastern and western boundaries of each sector. Specifically, we assign the zonal transport of water out of sector i through its eastern edge using the mean velocity in the same sector, and the transport in through its western edge using the mean velocity in sector $i - 1$, that is, from the west. A consistent approximation for the geostrophic meridional flow is obtained using the mean pressure difference between sectors i and $i - 1$. This yields a multibasin generalization of the isopycnal height equation (A8):

$$\frac{\partial z_i}{\partial t} - \frac{1}{L_i}(\Psi_i - \Psi_{i-1}) - \frac{\partial \psi_i}{\partial y} = -\frac{\partial}{\partial b}\left[\kappa_i\left(\frac{\partial z_i}{\partial b}\right)^{-1} + B_i\right], \tag{A14}$$

where

$$\psi_i = -\frac{\tau_i}{\rho_0 f} + K_i\frac{\partial z_i}{\partial y} + \frac{1}{\rho_0 f L_i}\int_{z_i}^0 (\overline{p}_i - \overline{p}_{i-1})dz'. \tag{A15}$$

APPENDIX B

Analytical Solution of the Adiabatic Two-Basin Residual-Mean Equations

This appendix provides the solution to the steady, adiabatic, two-basin, residual-mean equations with linear vertical shear and uniform surface wind stress and eddy diffusivity, given by (23a)–(23b). Taking a weighted zonal average of (23a) and (23b) yields an equation for the circumpolar-mean isopycnal depth ζ:

$$\frac{d\psi}{dy} = \frac{d}{dy}\left(-\frac{\tau}{\rho_0 f} + K\frac{d\zeta}{dy}\right) = 0. \tag{B1}$$

The weighted zonal average has canceled all terms associated with zonal convergence/divergence of mass by the flow of the ACC, so we recover the residual-mean equation derived in the adiabatic limit by Marshall and Radko (2003). The circumpolar-averaged residual streamfunction

$$\psi = \frac{L_A\psi_A + L_P\psi_P}{L_A + L_P} = -\frac{\tau}{\rho_0 f} + K\frac{d\zeta}{dy} \tag{B2}$$

is constant along buoyancy surfaces. We may therefore treat this streamfunction as a function of b alone, $\psi = \psi(b)$, and solve (B1) to obtain

$$\zeta = \zeta_0 + \left(\frac{\psi}{K} + \frac{\tau}{\rho_0 f\, K}\right)y. \tag{B3}$$

Here, $y = 0$ corresponds to the northern edge of the circumpolar channel, and $\zeta_0 = \zeta|_{y=0}$ is the isopycnal depth there. It follows from the boundary conditions of (24) that $\psi = 0$ on this isopycnal, so (B3) simplifies to

$$\zeta = \zeta_0 + sy. \tag{B4}$$

Intuitively, the residual streamfunction vanishes on this isopycnal because in a circumpolar average the net flux above and below the isopycnal is zero, the result of large, oppositely directed meridional mass fluxes in the two basins. Here, we define $s = \tau/\rho_0 fK$ as the constant circumpolar-averaged slope of this isopycnal.

If we instead subtract (23b) from (23a), we obtain an equation for Δ, the difference in the isopycnal depth between the two basins:

$$\frac{d^2\Delta}{dy^2} = \left(\frac{1}{L_A} + \frac{1}{L_P}\right)\Delta\left(U + \frac{1}{2}U_z\zeta\right). \tag{B5}$$

As we have an explicit solution for $\zeta(y)$, (B5) is a closed, one-dimensional, ordinary, differential equation for Δ. To solve, we define a modified latitudinal coordinate

$$Y = \frac{y_0 - y}{\lambda}, \tag{B6}$$

where

$$y_0 = \frac{2U}{(-s)U_z} - \frac{\zeta_0}{s}, \quad \lambda^3 = \frac{2K}{(-s)U_z(1/L_A + 1/L_P)}, \tag{B7}$$

are a reference latitude and characteristic length scale, respectively. Recall that the slope s is negative, so the length scale λ is real valued. Substituting (B6) and (B7) into (B5) yields

$$\frac{d^2\Delta}{dY^2} = \Delta Y, \tag{B8}$$

which is the canonical Airy equation with general solution

$$\Delta = \alpha \mathrm{Ai}(Y) + \beta \mathrm{Bi}(Y). \tag{B9}$$

Here, Ai and Bi are the Airy functions of the first and second kinds, respectively (Abramowitz and Stegun 1964), and α and β are arbitrary constants. To determine α and β, we use (A15) to rewrite (24) and (25) as a pair of boundary conditions for the isopycnal depth difference Δ:

$$\frac{\partial \Delta}{\partial y} = 0 \quad \text{at} \quad y = -l, \quad \text{and} \tag{B10}$$

$$\frac{\partial \Delta}{\partial y} = \frac{T}{K}\left(\frac{1}{L_A} + \frac{1}{L_P}\right) \quad \text{at} \quad y = 0. \tag{B11}$$

Substituting these conditions into (B9) allows us to solve for α and β and yields the following solution for Δ:

$$\Delta(y) = \frac{T\lambda}{K}\left(\frac{1}{L_A} + \frac{1}{L_P}\right) \times \frac{\mathrm{Bi}\left(\frac{y_0 - y}{\lambda}\right)\mathrm{Ai}'\left(\frac{y_0 + l}{\lambda}\right) - \mathrm{Ai}\left(\frac{y_0 - y}{\lambda}\right)\mathrm{Bi}'\left(\frac{y_0 + l}{\lambda}\right)}{\mathrm{Bi}'\left(\frac{y_0 + l}{\lambda}\right)\mathrm{Ai}'\left(\frac{y_0}{\lambda}\right) - \mathrm{Ai}'\left(\frac{y_0 + l}{\lambda}\right)\mathrm{Bi}'\left(\frac{y_0}{\lambda}\right)}, \tag{B12}$$

where Ai′ and Bi′ are the first derivatives of Ai and Bi, respectively. Note that we can recover the isopycnal depths in the Atlantic and Pacific sectors via

$$z_A = \zeta + \frac{L_P}{L_A + L_P}\Delta, \quad z_P = \zeta - \frac{L_A}{L_A + L_P}\Delta. \tag{B13}$$

Though exact, solution (B12) yields little insight into the interbasin differences in stratification due to its complicated form. A simpler solution can be derived via the same method when the change in zonal velocity along the isopycnal is small: $U_z l/U|s| \ll 1$. In this case, the term proportional to U_z in (B5) can be neglected, and the solution for Δ simplifies to

$$\Delta = \frac{T\Lambda}{K}\left(\frac{1}{L_A} + \frac{1}{L_P}\right)\frac{\cosh[(y + l)/\Lambda]}{\sinh(l/\Lambda)}. \tag{B14}$$

Here, the characteristic length scale has been modified to

$$\Lambda = \sqrt{\frac{K/U}{1/L_A + 1/L_P}}. \tag{B15}$$

For representative values of $K = 1000\,\mathrm{m^2\,s^{-1}}$, $U = 0.1\,\mathrm{m\,s^{-1}}$, $L_p = 10\,000\,\mathrm{km}$, and $L_A = 5000\,\mathrm{km}$, we obtain $\Lambda \approx 183\,\mathrm{km}$. This is much smaller than the width of the ACC, $\Lambda/l \ll 1$, so we can approximately simplify (B14) to

$$\Delta \approx \frac{T\Lambda}{K}\left(\frac{1}{L_A} + \frac{1}{L_P}\right)e^{y/\Lambda}. \tag{B16}$$

REFERENCES

Abernathey, R., J. Marshall, and D. Ferreira, 2011: The dependence of Southern Ocean meridional overturning on wind stress. *J. Phys. Oceanogr.*, **41**, 2261–2278, doi:10.1175/JPO-D-11-023.1.

Abramowitz, M., and I. A. Stegun, 1964: *Handbook of Mathematical Functions with Formulas, Graphs, and Mathematical Tables*. Applied Mathematics Series, Vol. 55, U.S. Government Printing Office, 1046 pp.

Aoki, S., S. R. Rintoul, S. Ushio, S. Watanabe, and N. L. Bindoff, 2005: Freshening of the Adélie Land Bottom Water near 140°E. *Geophys. Res. Lett.*, **32**, L23601, doi:10.1029/2005GL024246.

Bishop, S. P., P. Gent, F. Bryan, A. Thompson, M. Long, and R. Abernathey, 2016: Southern Ocean overturning compensation in an eddy-resolving climate simulation. *J. Phys. Oceanogr.*, **46**, 1575–1592, doi:10.1175/JPO-D-15-0177.1.

Broecker, W. S., 1991: The great ocean conveyor. *Oceanography*, **4**, 79–89, doi:10.5670/oceanog.1991.07.

Bryan, K., and L. J. Lewis, 1979: A water mass model of the world ocean. *J. Geophys. Res.*, **84**, 2503–2517, doi:10.1029/JC084iC05p02503.

Burke, A., A. L. Stewart, J. F. Adkins, R. Ferrari, M. F. Jansen, and A. F. Thompson, 2015: The glacial mid-depth radiocarbon bulge and its implications for the overturning circulation. *Paleoceanography*, **30**, 1021–1039, doi:10.1002/2015PA002778.

Cerovečki, I., M. R. Mazloff, and L. D. Talley, 2011: A comparison of Southern Ocean air–sea buoyancy flux from an ocean state estimate with five other products. *J. Climate*, **24**, 6283–6306, doi:10.1175/2011JCLI3858.1.

Curry, W. B., and D. W. Oppo, 2005: Glacial water mass geometry and the distribution of $\delta^{13}C$ of $\sum CO_2$ in the western Atlantic Ocean. *Paleoceanography*, **20**, PA1017, doi:10.1029/2004PA001021.

Dufour, C. O., and Coauthors, 2015: Role of mesoscale eddies in cross-frontal transport of heat and biogeochemical tracers in the Southern Ocean. *J. Phys. Oceanogr.*, **45**, 3057–3081, doi:10.1175/JPO-D-14-0240.1.

Ferrari, R., M. Jansen, J. F. Adkins, A. Burke, A. L. Stewart, and A. F. Thompson, 2014: An ocean tale of two climates: Modern and Last Glacial Maximum. *Proc. Natl. Acad. Sci. USA*, **111**, 8753–8758, doi:10.1073/pnas.1323922111.

Fukamachi, Y., S. R. Rintoul, J. A. Church, S. Aoki, S. Sokolov, M. A. Rosenberg, and M. Wakatsuchi, 2010: Strong export of Antarctic Bottom Water east of the Kerguelen Plateau. *Nat. Geosci.*, **3**, 327–331, doi:10.1038/ngeo842.

Gent, P. R., and J. C. McWilliams, 1990: Isopycnal mixing in ocean circulation models. *J. Phys. Oceanogr.*, **20**, 150–155, doi:10.1175/1520-0485(1990)020<0150:IMIOCM>2.0.CO;2.

Gnanadesikan, A., 1999: A simple predictive model of the structure for the oceanic pycnocline. *Science*, **283**, 2077–2079, doi:10.1126/science.283.5410.2077.

Goodwin, P., 2012: An isopycnal box model with predictive deep-ocean structure for biogeochemical cycling applications. *Ocean Modell.*, **51**, 19–36, doi:10.1016/j.ocemod.2012.04.005.

Gouretski, V. V., and K. P. Koltermann, 2004: WOCE Global Hydrographic Climatology: A technical report. Berichte des Bundesamtes für Seeschifffahrt und Hydrographie 35/2004, 52 pp.

Ito, T., and J. Marshall, 2008: Control of lower-limb overturning circulation in the Southern Ocean by diapycnal mixing and mesoscale eddy transfer. *J. Phys. Oceanogr.*, **38**, 2832–2845, doi:10.1175/2008JPO3878.1.

Jacobs, S. S., A. F. Amos, and P. M. Bruchausen, 1970: Ross Sea oceanography and Antarctic Bottom Water formation. *Deep-Sea Res. Oceanogr. Abstr.*, **17**, 935–962, doi:10.1016/0011-7471(70)90046-X.

Jones, C. S., and P. Cessi, 2016: Interbasin transport of the meridional overturning circulation. *J. Phys. Oceanogr.*, **46**, 1157–1169, doi:10.1175/JPO-D-15-0197.1.

Large, W. G., and S. G. Yeager, 2009: The global climatology of an interannually varying air–sea flux data set. *Climate Dyn.*, **33**, 341–364, doi:10.1007/s00382-008-0441-3.

Ledwell, J. R., A. J. Watson, and C. S. Law, 1993: Evidence for slow mixing across the pycnocline from an open-ocean tracer-release experiment. *Nature*, **364**, 701–703, doi:10.1038/364701a0.

LeVeque, R. J., 2002: *Finite Volume Methods for Hyperbolic Problems*. Cambridge University Press, 558 pp.

Lumpkin, R., and K. Speer, 2007: Global ocean meridional overturning. *J. Phys. Oceanogr.*, **37**, 2550–2562, doi:10.1175/JPO3130.1.

Lund, D. C., J. F. Adkins, and R. Ferrari, 2011: Abyssal Atlantic circulation during the Last Glacial Maximum: Constraining the ratio between transport and vertical mixing. *Paleoceanography*, **26**, PA1213, doi:10.1029/2010PA001938.

Marshall, D. P., 1997: Subduction of water masses in an eddying ocean. *J. Mar. Res.*, **55**, 201–222, doi:10.1357/0022240973224373.

Marshall, J., and T. Radko, 2003: Residual-mean solutions for the Antarctic Circumpolar Current and its associated overturning circulation. *J. Phys. Oceanogr.*, **33**, 2341–2354, doi:10.1175/1520-0485(2003)033<2341:RSFTAC>2.0.CO;2.

——, and ——, 2006: A model of the upper branch of the meridional overturning of the Southern Ocean. *Prog. Oceanogr.*, **70**, 331–345, doi:10.1016/j.pocean.2006.07.004.

——, and K. Speer, 2012: Closure of the meridional overturning circulation through Southern Ocean upwelling. *Nat. Geosci.*, **5**, 171–180, doi:10.1038/ngeo1391.

Mazloff, M. R., R. Ferrari, and T. Schneider, 2013: The force balance of the Southern Ocean meridional overturning circulation. *J. Phys. Oceanogr.*, **43**, 1193–1208, doi:10.1175/JPO-D-12-069.1.

McDougall, T. J., and P. C. McIntosh, 2001: The temporal-residual-mean velocity. Part II: Isopycnal interpretation and the tracer and momentum equations. *J. Phys. Oceanogr.*, **31**, 1222–1246, doi:10.1175/1520-0485(2001)031<1222:TTRMVP>2.0.CO;2.

McIntosh, P. C., and T. J. McDougall, 1996: Isopycnal averaging and the residual mean circulation. *J. Phys. Oceanogr.*, **26**, 1655–1660, doi:10.1175/1520-0485(1996)026<1655:IAATRM>2.0.CO;2.

Morrison, A. K., and A. M. Hogg, 2013: On the relationship between Southern Ocean overturning and ACC transport. *J. Phys. Oceanogr.*, **43**, 140–148, doi:10.1175/JPO-D-12-057.1.

——, ——, and M. L. Ward, 2011: Sensitivity of the Southern Ocean overturning circulation to surface buoyancy forcing. *Geophys. Res. Lett.*, **38**, L14602, doi:10.1029/2011GL048031.

Munday, D. R., H. L. Johnson, and D. P. Marshall, 2013: Eddy saturation of equilibrated circumpolar currents. *J. Phys. Oceanogr.*, **43**, 507–532, doi:10.1175/JPO-D-12-095.1.

Munk, W. H., 1966: Abyssal recipes. *Deep-Sea Res. Oceanogr. Abstr.*, **13**, 707–730, doi:10.1016/0011-7471(66)90602-4.

Naveira Garabato, A. C., R. Ferrari, and K. L. Polzin, 2011: Eddy stirring in the Southern Ocean. *J. Geophys. Res.*, **116**, C09019, doi:10.1029/2010JC006818.

——, A. P. Williams, and S. Bacon, 2014: The three-dimensional overturning circulation of the Southern Ocean during the WOCE era. *Prog. Oceanogr.*, **120**, 41–78, doi:10.1016/j.pocean.2013.07.018.

Nikurashin, M., and G. Vallis, 2011: A theory of deep stratification and overturning circulation in the ocean. *J. Phys. Oceanogr.*, **41**, 485–502, doi:10.1175/2010JPO4529.1.

——, and ——, 2012: A theory of the interhemispheric meridional overturning circulation and associated stratification. *J. Phys. Oceanogr.*, **42**, 1652–1667, doi:10.1175/JPO-D-11-0189.1.

Ohshima, K. I., and Coauthors, 2013: Antarctic Bottom Water production by intense sea-ice formation in Cape Darnley polynya. *Nat. Geosci.*, **6**, 235–240, doi:10.1038/ngeo1738.

Orsi, A. H., and T. Whitworth, 2005: *Southern Ocean.* Vol. 1, *Hydrographic Atlas of the World Ocean Circulation Experiment (WOCE)*, WOCE International Project Office, 223 pp.

——, ——, and W. D. Nowlin Jr., 1995: On the meridional extent and fronts of the Antarctic Circumpolar Current. *Deep-Sea Res. I*, **42**, 641–673, doi:10.1016/0967-0637(95)00021-W.

Radko, T., and J. Marshall, 2006: The Antarctic Circumpolar Current in three dimensions. *J. Phys. Oceanogr.*, **36**, 651–669, doi:10.1175/JPO2893.1.

——, and I. Kamenkovich, 2011: Semi-adiabatic model of the deep stratification and meridional overturning. *J. Phys. Oceanogr.*, **41**, 757–780, doi:10.1175/2010JPO4538.1.

Reid, J. L., 1961: On the temperature, salinity and density differences between the Atlantic and Pacific Oceans in the upper kilometre. *Deep-Sea Res.*, **7**, 265–275, doi:10.1016/0146-6313(61)90044-2.

Sallée, J.-B., R. J. Matear, S. R. Rintoul, and A. Lenton, 2012: Localized subduction of anthropogenic carbon dioxide in the Southern Hemisphere oceans. *Nat. Geosci.*, **5**, 579–584, doi:10.1038/ngeo1523.

Shakespeare, C. J., and A. M. Hogg, 2012: An analytical model of the response of the meridional overturning circulation to changes in wind and buoyancy forcing. *J. Phys. Oceanogr.*, **42**, 1270–1287, doi:10.1175/JPO-D-11-0198.1.

Speer, K., S. R. Rintoul, and B. Sloyan, 2000: The diabatic Deacon cell. *J. Phys. Oceanogr.*, **30**, 3212–3222, doi:10.1175/1520-0485(2000)030<3212:TDDC>2.0.CO;2.

Sprintall, J., and A. Révelard, 2014: The Indonesian Throughflow response to Indo-Pacific climate variability. *J. Geophys. Res. Oceans*, **119**, 1161–1175, doi:10.1002/2013JC009533.

Stewart, A. L., and A. F. Thompson, 2013: Connecting Antarctic cross-slope exchange with Southern Ocean overturning. *J. Phys. Oceanogr.*, **43**, 1453–1471, doi:10.1175/JPO-D-12-0205.1.

——, R. Ferrari, and A. F. Thompson, 2014: On the importance of surface forcing in conceptual models of the deep ocean. *J. Phys. Oceanogr.*, **44**, 891–899, doi:10.1175/JPO-D-13-0206.1.

Su, Z., A. L. Stewart, and A. F. Thompson, 2014: An idealized model of Weddell Gyre export variability. *J. Phys. Oceanogr.*, **44**, 1671–1688, doi:10.1175/JPO-D-13-0263.1.

Talley, L. D., 2013: Closure of the global overturning circulation through the Indian, Pacific, and Southern Oceans: Schematics and transports. *Oceanography*, **26**, 80–97, doi:10.5670/oceanog.2013.07.

Tamsitt, V., L. D. Talley, M. R. Mazloff, and I. Cerovečki, 2016: Zonal variations in the Southern Ocean heat budget. *J. Climate*, doi:10.1175/JCLI-D-15-0630.1, in press.

Thompson, A. F., and J.-B. Sallée, 2012: Jets and topography: Jet transitions and the impact on transport in the Antarctic Circumpolar Current. *J. Phys. Oceanogr.*, **42**, 956–972, doi:10.1175/JPO-D-11-0135.1.

——, and A. C. N. Garabato, 2014: Equilibration of the Antarctic Circumpolar Current by standing meanders. *J. Phys. Oceanogr.*, **44**, 1811–1828, doi:10.1175/JPO-D-13-0163.1.

Toggweiler, J. R., and B. Samuels, 1995: Effect of Drake Passage on the global thermohaline circulation. *Deep-Sea Res. II*, **42**, 477–500, doi:10.1016/0967-0637(95)00012-U.

Wolfe, C. L., and P. Cessi, 2010: What sets the strength of the middepth stratification and overturning circulation in eddying ocean models? *J. Phys. Oceanogr.*, **40**, 1520–1538, doi:10.1175/2010JPO4393.1.

——, and ——, 2014: Salt feedback in the adiabatic overturning circulation. *J. Phys. Oceanogr.*, **44**, 1175–1194, doi:10.1175/JPO-D-13-0154.1.

Wyrtki, K., 1987: Indonesian Throughflow and the associated pressure gradient. *J. Geophys. Res.*, **92**, 12 941–12 946, doi:10.1029/JC092iC12p12941.